

~~CONFIDENTIAL~~Copy
RM L50G18a

Inactive

~~NACA~~**RESEARCH MEMORANDUM**

SUMMARY OF THE AERODYNAMIC CHARACTERISTICS AND
FLYING QUALITIES OBTAINED FROM FLIGHTS OF ROCKET-PROPELLED
MODELS OF AN AIRPLANE CONFIGURATION INCORPORATING

A SWEEPBACK INVERSELY TAPERED WING AT
TRANSONIC AND LOW-SUPERSONIC SPEEDS

By Grady L. Mitcham and Willard S. Blanchard, Jr.

Langley Aeronautical Laboratory
~~CLASSIFICATION CANCELLED~~
Langley Air Force Base, Va.

Authority Date

By See

CLASSIFIED DOCUMENT

This document contains classified information affecting the National Defense of the United States within the meaning of the Espionage Act, USC 8031 and 32. Its transmission or the revelation of its contents in any manner to an unauthorized person is prohibited by law.
Information so classified may be imparted only to persons in the military and naval services of the United States, appropriate civilian officers and employees of the Federal Government who have a legitimate interest therein, and to United States citizens of known loyalty and discretion who of necessity must be informed thereof.

**NATIONAL ADVISORY COMMITTEE
FOR AERONAUTICS**

WASHINGTON

September 7, 1950

~~CONFIDENTIAL~~

NACA RM L50G18a



NATIONAL ADVISORY COMMITTEE FOR AERONAUTICS

RESEARCH MEMORANDUM

SUMMARY OF THE AERODYNAMIC CHARACTERISTICS AND
FLYING QUALITIES OBTAINED FROM FLIGHTS OF ROCKET-PROPELLED
MODELS OF AN AIRPLANE CONFIGURATION INCORPORATING
A SWEPTBACK INVERSELY TAPEDED WING AT
TRANSONIC AND LOW-SUPERSONIC SPEEDS

By Grady L. Mitcham and Willard S. Blanchard, Jr.

SUMMARY

Flight tests have been conducted on rocket-propelled models of an airplane configuration incorporating a sweptback wing with inverse taper to investigate the drag, stability, and control characteristics at transonic and supersonic speeds. The models were tested with a conventional tail arrangement in the Mach number range from 0.55 to 1.2. In addition to the various aerodynamic parameters obtained, the flying qualities were computed for a full-scale airplane with the center-of-gravity location at 18 percent of the mean aerodynamic chord. Also included in this investigation are drag measurements made on relatively simple fixed-control models tested with both conventional and V-tail arrangements. The results obtained from the models utilizing the V-tail arrangement have been presented in a previous paper (NACA RM L8G29).

The models tested with conventional tail arrangements gave higher values of minimum drag coefficient than the models with the V-tail assembly for Mach numbers from 0.55 to 1.15.

The variation of lift-curve slope with Mach number was smooth. Buffeting occurred at subsonic speeds as the models approached the maximum lift coefficient during abrupt pull-ups but was not evident elsewhere in the range investigated. The high range of lift coefficients was obtained only at subsonic speeds with the maximum being about 0.75. At supersonic speeds, the range of lift coefficients covered was limited by a large reduction in control effectiveness. The aerodynamic-center location differed for positive and negative lift coefficients below a Mach number of 1.0. The most-forward aerodynamic-center location of 23 percent of the mean aerodynamic chord occurred at a Mach number of 0.8 and the

most-rearward location of 52 percent occurred at a Mach number of 1.2. The airplane should trim at positive lift coefficients throughout the transonic speed range with the center-of-gravity location at 18 percent of the mean aerodynamic chord and the stabilizer set at 0° incidence. The maneuverability of the airplane would be limited in the transonic speed range at high altitudes as a result of the large reduction in control effectiveness at transonic speeds. The high stick forces at transonic and supersonic speeds will necessitate the airplane's being equipped with some type of control-boost system. The damping of the short-period longitudinal oscillation is adequate at sea level but is reduced at altitude.

INTRODUCTION

The National Advisory Committee for Aeronautics has conducted flight tests of rocket-powered models of an airplane configuration employing a sweptback wing with inverse taper to evaluate stability, control effectiveness, and drag at transonic and low-supersonic speeds. Three of the models were flown with a conventional tail arrangement and two were flown with a V-tail. This paper contains a summary of the results obtained from the flight tests of these models which were flown at the Langley Pilotless Aircraft Research Station, Wallops Island, Va.

Two of the models, both with the conventional tail arrangement, were flown with a programmed type of control which called for abrupt up and down movement of the elevators as the model traversed the speed range. The tests of these two models were conducted to measure lift, drag, pitching moments, damping in pitch, and control effectiveness at transonic speeds. This paper contains the basic aerodynamic parameters and the stability derivatives determined from the response of the models to the elevator motion and the results of an analysis of the flying qualities that might be expected from such an airplane at transonic and supersonic speeds.

The remaining three models were flown with the controls undeflected and were similar to the types used in reference 1 to investigate trim changes and drag through the transonic speed range. Results from two of the models are presented in reference 2. Drag results from the third model are presented in this paper in addition to the drag results taken from reference 2. Aileron rolling effectiveness was investigated by another technique and those results are given in reference 3.

SYMBOLS

t	time from launching, seconds
R	Reynolds number $\left(\frac{\rho V \bar{c}}{\mu}\right)$
V	velocity, feet per second
V _c	velocity of sound, feet per second
p	free-stream static pressure, pounds per square foot
γ	specific-heat ratio, value taken 1.40
q	dynamic pressure, pounds per square foot $\left(\frac{\gamma p M^2}{2}\right)$
ρ	mass density of air, slugs per cubic foot
W	weight of model, pounds
S	wing area, square feet
\bar{c}	mean aerodynamic chord, feet
a _l /g	longitudinal accelerometer reading
a _n /g	normal accelerometer reading
g	acceleration due to gravity, 32.2 feet per second per second
δ	elevator deflection measured normal to hinge line, degrees
C _C	chord-force coefficient $\left(\frac{a_l}{g} \frac{W}{S} \frac{1}{q}\right)$
C _N	normal-force coefficient $\left(\frac{a_n}{g} \frac{W}{S} \frac{1}{q}\right)$
C _L	lift coefficient $(C_N \cos \alpha + C_C \sin \alpha)$
C _D	drag coefficient $(C_N \sin \alpha - C_C \cos \alpha)$

C_m	pitching-moment coefficient about center of gravity
$C_{L\alpha}$	rate of change of lift coefficient with angle of attack at constant elevator deflection, per degree
α	angle of attack, degrees
α_{trim}	trim angle of attack, degrees
δ_{trim}	trim elevator deflection, degrees
$C_{L_{trim}}$	trim lift coefficient
$C_{L\delta_{trim}}$	rate of change of trim lift coefficient with elevator deflection, per degree
$C_{L\delta}$	rate of change of lift coefficient with elevator deflection at constant angle of attack, per degree
$\left(\frac{\Delta\alpha}{\Delta\delta}\right)_{trim}$	rate of change of angle of attack with elevator deflection between two trim conditions
C_h	hinge-moment coefficient $\left(\frac{\text{Hinge moment about hinge line}}{qb_e\bar{c}_e^2}\right)$
b_e	elevator span along hinge line
\bar{c}_e	elevator root-mean-square chord perpendicular to hinge line
$\frac{\Delta C_h}{\Delta\delta}$	increment of hinge-moment coefficient due to elevator deflection, per degree
$C_{m\alpha}$	rate of change of pitching-moment coefficient with angle of attack, per degree
$C_{m\delta}(\alpha=K)$	rate of change of pitching-moment coefficient with elevator deflection for constant angle of attack, per degree
C_{m_0}	pitching-moment coefficient at zero angle of attack and zero elevator deflection
I_y	moment of inertia about pitch axis, slug-feet ²

P	period of short-period longitudinal oscillation, seconds
$T_{1/2}$	time to damp to one-half amplitude, seconds
$C_{1/10}$	cycles for the short-period oscillation to damp to one-tenth amplitude
A	wing aspect ratio
m	mass of model, slugs
$C_{m_{\dot{\theta}} \bar{c}} = \frac{\partial C_m}{\partial \frac{\dot{\theta} \bar{c}}{2V}}$	per radian
$C_{m_{\dot{\alpha}} \bar{c}} = \frac{\partial C_m}{\partial \frac{\dot{\alpha} \bar{c}}{2V}}$	per radian
θ	pitch angle
$\dot{\theta}$	derivative of θ with respect to time, radians per second
$\dot{\alpha}$	derivative of α with respect to time, radians per second

MODELS AND APPARATUS

Models

Pulsed-control models.- Figure 1 presents a three-view drawing showing the principal dimensions of the models used in the stability and control investigation and table I gives the principal geometric characteristics of the models and the full-size airplane; the weight and balance data are given in table II. The pulsed-control models are referred to as models 1 and 2 in this paper. Wing airfoil ordinates are presented in table III. Photographs of these models are shown as figure 2.

The fuselages were of all-metal construction of the monocoque type divided into three sections; the nose section which held the

[REDACTED]

telemeter and batteries, the center section which held the wings and the compressed-air supply for the control-actuating system, and the tail section which contained the control-actuating system and the tail assembly.

The programmed movement of the elevators was accomplished by a compressed-air system which called for abrupt up and down deflections operating at a frequency of about 1 cycle per second. The elevators, which were unsealed, moved together between stops in an approximately square-wave motion. On model 1, the controls were set under static no-load conditions so that the elevator would be deflected up 0° and down 8° ; on model 2 the deflections were up 11.0° and down 0° . Prior to each flight a known static load was applied at a point at about the middle of the span of the elevator and the deflection at the root and midspan were measured; this calibration was used to correct the control positions recorded during the flight tests to an average spanwise value.

Since the pulsed-control models contained no internal propulsion system, they were boosted to supersonic speeds by a solid-fuel, 6-inch-diameter Deacon rocket motor capable of producing an average thrust of 6500 pounds for approximately 3.1 seconds.

At cessation of the booster rocket thrust the booster was separated from the model by drag inasmuch as the drag-weight ratio of the model was less than the drag-weight ratio of the booster.

The booster-model combinations were ground launched from a crutch type of launcher as shown in figure 3. The launching angle from the horizontal was 45° . Figure 4 shows a sequence of photographs of one of the booster-model combinations at take-off.

Fixed-control models. - Two models with a V-tail arrangement, models B and C, and one with a conventional tail, model D, were flown with 0° stabilizer incidence and the elevators fixed at 0° deflection. A three-view drawing of the models with the V-tail arrangement is shown in figure 5. Model D was the same as models B and C except for the tail. Photographs of the models are shown as figures 6 and 7. Areas and dimensions of the models are presented in table I.

Apparatus

The data from the flights were obtained by the use of Doppler velocimeter radar, tracking radar, telemeters, photography, and radio-sondes. The models were tracked in flight by a Doppler velocimeter radar unit to evaluate velocity along the flight path and by a tracking radar unit to determine the trajectory.

The time histories of the data as the models traversed the Mach number range were transmitted and recorded by a telemeter system which gave two channels of continuous information on the fixed-control models and six continuous channels of information on the pulsed-control models. Longitudinal and normal acceleration were recorded on the fixed-control models and data recorded on the pulsed models were longitudinal acceleration, normal acceleration, control position, angle of attack, total pressure, and a reference static pressure. On the pulsed-control models, angles of attack were obtained by a vane-type angle-of-attack indicator (reference 4) located on a sting ahead of the nose of the model. The range of angles of attack covered by this vane-type indicator was approximately $\pm 15^\circ$. Motion-picture cameras recorded the flights and launchings.

The values of temperature and static pressure used in calculating density and speed of sound were obtained from radiosonde observations made at the time of firing. The methods for obtaining velocity are described in references 5 and 6.

METHODS OF ANALYSIS

In both fixed- and pulsed-control techniques all the data were obtained during the decelerating part of the flight. The methods of analysis used in reducing the data from the pulsed-control models apply to the free oscillation resulting from a step-function disturbance. This disturbance was created by pulsing the elevators up and down in approximate square-wave motion at the rate of about 1 cycle per second, which produced corresponding changes in angle of attack and normal acceleration. The longitudinal stability was indicated by the period and rate of decay of the short-period longitudinal oscillations during the period when the controls were held fixed between pulses. The analysis of these longitudinal oscillations is based on two degrees of freedom, translation normal to the flight path and rotation in pitch about the center of gravity. To simplify the analysis and to permit the determination of equations for the more important aerodynamic derivatives, two further assumptions are necessary. It is assumed that during the time interval over which each calculation is made the forward velocity is constant and the aerodynamic forces and moments vary linearly with $\dot{\alpha}$, α , θ , $\dot{\theta}$, and δ . The complete derivation of the equations used is not given herein, but the equations are shown in the form that was used; they are

$$mV(\dot{\theta} - \alpha) = (C_{L\alpha}\alpha + C_{L\delta}\delta)qS \quad (1)$$

$$I_y \ddot{\theta} = qS\bar{c} \left(C_{m\alpha} \alpha + C_{m_{\dot{\alpha}\bar{c}}} \frac{\dot{\alpha}\bar{c}}{2V} + C_{m_{\dot{\theta}\bar{c}}} \frac{\dot{\theta}\bar{c}}{2V} + C_{m\delta} \delta \right) \quad (2)$$

A more complete discussion of the methods and corrections used in reducing these data from the time-history records to the parameters presented in this paper is given in the appendixes of references 5 and 6.

The Reynolds numbers of all the models and the assumed full-scale airplane based on the mean aerodynamic chord are shown in figure 8.

RESULTS AND DISCUSSION

Aerodynamic Coefficients and Stability Derivatives

Lift characteristics. - The lift characteristics of models 1 and 2 are shown in figures 9, 10, and 11. Lift coefficients at constant angles of attack as a function of Mach number and the elevator deflections at which they occurred are presented in figure 9. As can be seen from this figure, the range of lift coefficients covered at high speeds was small; this was the result of the reduced control effectiveness. Model 1 was flown at mostly negative lift coefficients with a few values of positive C_L being obtained at subsonic speeds, and model 2 was flown at positive lift coefficients. Between $M = 0.62$ and $M = 0.67$ values for both positive and negative lift coefficients were obtained from model 1. Figure 10 presents these values of lift coefficient at various angles of attack. The data indicate some nonlinearity of the lift curves between positive and negative lift coefficients. This nonlinearity is consistent with the curves in figure 11, which gives the variation of lift-curve slopes with Mach number. This figure shows that the lift-curve slope was consistently higher in the negative-lift range than in the positive-lift range.

Maximum lift coefficient. - Figure 12 shows the maximum lift coefficients reached in these tests, as obtained from model 2. At Mach numbers below 0.72 the model apparently was approaching maximum lift each time it oscillated to a positive angle of attack following a negative control deflection. The Reynolds number at these Mach numbers corresponded to about 13,000,000.

Buffet boundary. - On model 2, the model flown at positive lift coefficients, buffeting occurred at high lift coefficients below $M = 0.78$. No values of lift coefficients above $C_L = 0.65$ and no buffeting were recorded

above $M = 0.78$. However, due to the decrease in stability and the increased control effectiveness of the configuration, a higher range of lift coefficients was covered below $M = 0.78$. An illustrative section of the telemeter traces of normal acceleration and angle of attack at which buffet oscillation is apparent is shown in figure 13.

Prior to flight testing, the model was suspended by shock cords and shaken with two electromagnetic shakers at frequencies up to 400 cycles per second. A fundamental frequency of 59 cycles per second was observed from the six-channel telemeter record taken during the ground tests. Only the normal-acceleration channel showed any frequency response in the ground tests. These responses occurred at 59, 115, and 230 cycles per second and were attributed to the wings of the model whose amplitude of vibration showed a marked increase at these points in the frequency spectrum. From figure 13, it may be seen from the flight data that resonances at a frequency of about 60 cycles per second occurred in normal acceleration. Point A marks the beginning of the buffet oscillation and point B, the decay of the exciting force. Point B is more difficult to ascertain than point A since it represents the point where the exciting force stops; therefore, its location is not an exact point. The sinusoidal oscillation occurring between points B and C is believed to represent the free vibration of the wing. It may be seen that point B occurs at a lower C_L than point A; this same indication was obtained from flight tests on a full-scale airplane of a different configuration (reference 7). It may be noted that an abrupt change of elevator angle produced no resonant frequencies in the corresponding angle of attack or acceleration responses. Consequently this oscillation is believed to be buffeting due to high lift and not the result of sudden control movement.

Figure 14 shows the lift coefficients where buffeting starts and stops as a function of Mach number. It may be seen from figure 14 that the lift coefficient at which buffeting stops lies below the point where it initially started throughout the Mach number range where high lift coefficients were obtained.

Drag

The minimum drag coefficients obtained from the flights of the models tested with both V-tail (reference 2) and conventional tail (T-tail) arrangements are presented in figure 15. Models B and C (V-tail arrangement) indicate considerably lower drag than models D and 2 (conventional tail arrangement) which gave a value of $C_D = 0.065$ at $M = 1.15$. The magnitude of the difference between V- and T-tail models varied from ΔC_D of 0.006 at $M = 0.7$ to a ΔC_D of 0.016 at $M = 1.0$. The values for $C_{D_{min}}$ on the models with the conventional tail arrangement were obtained at approximately $C_L = 0.10$ and on the models with V-tails

at $C_L = \pm 0.02$. Several differences in the models used in the investigation, namely, tail plan form and area, shape of base section of fuselage, windshield-canopy arrangement, and model surface finish, contribute to the difference in drag. The fairings on the base sections of the fuselages of models B, C, and D differed from those on model 2, as shown in figures 1 and 5. However, the contribution of this difference in base fairings to C_D is believed to be small since the difference in $C_{D_{min}}$ obtained on model 2 and model D (models with same tail arrangement but different base fairings) is within the scatter of the results. The drag results presented in references 8 and 9 for research models with a flat windshield canopy (similar to canopies on models B, C, and D) and a V-windshield canopy (as on models 1 and 2) indicate the values of drag for the V-windshield to be slightly lower between $M = 0.85$ and $M = 1.2$. The surface finishes on models B, C, and D were noticeably smoother than on model 2. Since these incremental differences in drag appear to be a small contribution to the rather large differences in $C_{D_{min}}$ obtained from the models with V-tail and conventional tail arrangements, the higher drag for the conventional T-tail arrangement can only be attributed to differences in the tails and interference for the two tail arrangements or to error in the measurements.

The drag coefficients for model 2 for the lift-coefficient range from 0.1 to 0.7 are shown as a function of Mach number in figure 16. The range of C_L obtained at supersonic speeds was lower than that obtained at subsonic speeds because of the decreased elevator effectiveness and the increased stability of the configuration. These data were obtained from one of the pulsed-control models during the short-period oscillation resulting from abrupt pull-ups. The effect of lift on drag is also shown in figure 16. For a wing with the resultant force normal to the chord plane, dC_D/dC_L^2 should equal $1/C_{L\alpha}$; however, from figure 17 the test results for dC_D/dC_L^2 fall below the curve representing $1/C_{L\alpha}$ at Mach numbers below 0.95 and rise to coincide with this curve from $M = 0.95$ to $M = 1.15$. The difference at subsonic speeds shows that leading-edge suction is present, which can be expected from a sweptback wing with a round-nose airfoil.

Longitudinal Stability

Static stability.- The static stability of the configuration was determined from the measured periods of the short-period longitudinal oscillations obtained in angle of attack as a result of the disturbance created by the abrupt movement of the elevators.

The values of period obtained from the two models flown at different center-of-gravity locations are shown in figure 18. These data show a decrease in period in the transonic region and the expected gradual decrease with increasing speed at supersonic speeds. The absence of values of the period for model 1 between $M = 1.00$ and $M = 1.20$ was caused by an unreadable portion of the telemeter record. However, a reliable value was obtained at $M = 1.2$. These values of period were used to obtain the static-longitudinal-stability parameter $C_{m_{\dot{\alpha}}}$ which is presented as a function of Mach number in figure 19. From this figure it is evident that some nonlinearities exist in the variation of pitching moment with angle of attack for the two models.

The values of $C_{m_{\dot{\alpha}}}$ were used to compute aerodynamic-center location shown in figure 20. The dashed portion of the curve shown for model 1 is uncertain since $C_{L_{\dot{\alpha}}}$ was unknown above $M = 1.00$. However, since a value of $C_{m_{\dot{\alpha}}}$ was computed from a measured period at $M = 1.2$, $C_{L_{\dot{\alpha}}}$ was estimated and a value for aerodynamic-center location was obtained at $M = 1.2$. The aerodynamic center moves from its most-forward position of 23 percent mean aerodynamic chord at $M = 0.8$ to the most-rearward location of 52 percent mean aerodynamic chord at $M = 1.2$. The results obtained from the two models show good agreement at $M = 0.70$ and $M = 1.20$; however, at $M = 0.9$ the aerodynamic center is apparently a function of lift coefficient.

Dynamic stability.- The time required for the longitudinal short-period oscillation of the model to damp to one-half amplitude is shown in figure 21. However, since the flight-test models were not dynamic scale models, the results presented for $T_{1/2}$ are applicable to the full-scale airplane only; after corrections are applied as in references 5 and 6. The data converted to the total-damping factor $\frac{C_{m_{\dot{\alpha}}}}{2V} + \frac{C_{m_{\dot{\omega}}}}{2V}$ are given in figure 22. As indicated by these figures, there is a large increase in the damping-moment coefficients from subsonic to supersonic speeds.

Longitudinal Trim and Control Effectiveness

Longitudinal trim.- The longitudinal-trim characteristics of models 1 and 2 are shown in figures 23 and 24, respectively, and for models C and D in figure 25. It is apparent from these figures that the trim change throughout the transonic speed range was small. The values of trim lift coefficient $C_{L_{trim}}$, trim angle of attack α_{trim} , and trim elevator position δ_{trim} were determined from the time histories of model flights by the method described in reference 5. The apparent

zero-angle-of-attack pitching-moment coefficient C_{M_0} is shown for models 1 and 2 in figure 26. For model 2, C_{M_0} was approximately 0.01 more positive than for model 1. This is probably caused by slight variations in construction between the two models. Figure 26 indicates that at zero angle of attack the pitching moment increases with increasing Mach number.

Control effectiveness.- Figure 27 shows a plot of change in lift coefficient per degree of elevator deflection CL_{δ} at a constant angle of attack as a function of Mach number. The values of CL_{δ} are quite small, varying from a maximum value of 0.0047 at $M = 0.7$ to a minimum of 0.0019 at $M = 1.2$.

The change in trim lift coefficient with elevator deflection $CL_{\delta\text{trim}}$ is shown as a function of Mach number in figure 28 for models 1 and 2. For model 1 the values of $CL_{\delta\text{trim}}$ remained fairly constant up to $M = 0.85$ where an abrupt reduction from -0.041 to -0.013 occurred between $M = 0.85$ and $M = 1.00$. Values above $M = 1.00$ were not obtained on model 1. On model 2 the abrupt reduction of $CL_{\delta\text{trim}}$ from -0.051 to -0.015 occurred between $M = 0.83$ and $M = 0.94$ and remained relatively constant up to $M = 1.18$. It may be noted from figure 28 that the values of $CL_{\delta\text{trim}}$ obtained from model 1, the model with the most-forward center-of-gravity location, are lower than those obtained from model 2 at subsonic speeds but higher at transonic speeds. Due to the more forward center-of-gravity location on model 1, it would be expected that the values of $CL_{\delta\text{trim}}$ would be consistently lower than those obtained from model 2 throughout the Mach number range covered by the tests. This can be explained by the differences in aerodynamic-center location between the two models, which was the result of the difference between the lift-coefficient ranges covered by the tests.

The longitudinal-control effectiveness is also shown by figures 29 and 30; change in trim angle of attack per degree of elevator deflection $(\Delta\alpha/\Delta\delta)_{\text{trim}}$ and change in pitching-moment coefficient per degree of elevator deflection $C_{m_{\delta}}$ are both shown as functions of Mach number. There is an abrupt loss in the pitching moment supplied by the elevator from subsonic to supersonic speeds with a maximum value of -0.010 occurring at $M = 0.7$ and a minimum value of -0.004 occurring at $M = 1.18$.

The same effect is shown in figure 29. Since $(\frac{\Delta\alpha}{\Delta\delta})_{\text{trim}}$ is influenced by the stability of the configuration, the unusual variations between models 1 and 2 are believed to be a result of the nonlinearity of the pitching moments between positive and negative lift coefficients.

Hinge Moments

Some approximate values of hinge moments were reduced from these tests. The accuracy is less for the values obtained for hinge moments than for the other aerodynamic coefficients presented, since the hinge-moment characteristics were measured as a secondary factor. The flexibility of the control system was utilized in determining the hinge moments by measuring the amount by which the control linkage deflected under load. Figure 31 presents the hinge-moment results in the form of $\Delta C_h / \Delta \delta$ as a function of Mach number; these results include the $\Delta \alpha$ effects. Values of $C_{h\alpha}$ could not be determined from the change in elevator floating angle during the angle-of-attack oscillation following abrupt control deflections because of a slight amount of play in the system and because of the small values of angle of attack. Figure 31 shows that $\Delta C_h / \Delta \delta$ increases from a value of -0.007 at $M = 0.9$ to -0.017 at $M = 1.10$ and then gradually decreases to -0.015 at $M = 1.20$. The range of elevator deflection covered is given in figure 24.

Airplane Flying Qualities

The analysis of the flying qualities presented in the following section is based on an assumed full-scale airplane with the center-of-gravity location at 18 percent of the mean aerodynamic chord. The geometric and mass characteristics are given in tables I and II, respectively.

Longitudinal-trim characteristics.- The elevator angles required for trimmed level flight at sea level and 40,000 feet altitude are presented as a function of Mach number in figure 32. The rates of change of elevator angle required for level flight through the transonic region are sufficiently low at both sea level and 40,000 feet so that a pilot would experience no difficulty in maintaining level flight if it is assumed the stick forces are satisfactory. Due to the zero-angle-of-attack pitching-moment coefficient C_{m0} , the airplane would trim at positive lift coefficients (a pitching-up tendency) throughout the transonic region with elevator and stabilizer settings at 0° . For sea-level conditions, down elevator is required for level flight from $M = 0.75$ to $M = 1.18$; however, at 40,000 feet, up elevator is required for level flight as a result of the higher C_L required and the reduced control effectiveness at transonic speeds.

Figure 33 shows the variation of g at sea level and 40,000 feet as a function of Mach number for constant elevator deflection. At sea level, the airplane pitches up from $1g$ at $M = 0.80$ to about $2.8g$ at $M = 0.95$. At 40,000 feet, the airplane pitches down from $1g$

at $M = 0.80$ to about $0.7g$ at $M = 0.95$; thus, it can be concluded that the trim change at sea level and 40,000 feet is relatively mild.

The data from which these values were calculated were obtained from model 2, the model tested in the positive lift-coefficient range.

Longitudinal-control effectiveness.- The elevator effectiveness for the full-scale airplane, degrees of elevator deflection required for a change in normal acceleration of $1g$, $\Delta\delta/\Delta g$, is indicated in figure 34 as a function of Mach number. From this plot it is obvious that the control effectiveness of the airplane would be reduced by a large amount at transonic speeds, especially at high altitudes. For example, a $2g$ pull-up at 40,000 feet at $M = 0.95$ would require an up-elevator angle of approximately 24.5° . However, at $M = 0.75$ at an altitude of 40,000 feet the airplane would also be limited to about a $2g$ maneuver, unless some type of high-lift device was employed, since the results from the flight tests of the rocket-propelled models indicated the maximum lift coefficient to be approximately 0.75 at this Mach number.

Longitudinal control forces.- The stick forces presented in this analysis are based on a conventional airplane configuration with 2° of elevator deflection for 1 inch of stick movement. These stick forces were computed from the measured model hinge moments. Effect of angle of attack on the hinge moments was therefore only approximately accounted for. These data indicate the power required of a control-boost system with no balancing or trimming devices.

The elevator control force required for trim in straight and level flight at various Mach numbers is presented in figure 35 for sea-level flight and for flight at 40,000 feet. Stick force per g is presented in figure 36 as a function of Mach number. From these two figures it is apparent that the stick forces on such an airplane would be quite large at transonic and supersonic speeds.

Dynamic stability.- The U. S. Air Force specifications for stability and control characteristics of airplanes (reference 10) require that the short-period dynamic oscillation of normal acceleration produced by moving and quickly releasing the elevator shall be damped to $1/10$ amplitude in 1 cycle (based on free controls). The damping characteristics for this analysis have been evaluated for the control-fixed condition although there is a slight deflection in the control position due to hinge-moment effect and the flexibility of the control system. However, the control-fixed condition would dictate the behavior of this airplane, assuming an irreversible control-boost system is provided to aid the pilot in overcoming the large stick forces that would be encountered in maneuvering. The characteristics of the stick-fixed short-period longitudinal oscillations for the full-scale airplane are presented in

figures 37 to 39. Figure 37, which gives the cycles required to damp to 1/10 amplitude as a function of Mach number at sea level and 40,000 feet altitude, indicates that this airplane would meet the Air Force requirement for damping at sea level but would not conform to this requirement at 40,000 feet over the speed range covered by these tests.

The time required for the longitudinal short-period oscillation to damp to 1/2 amplitude as a function of Mach number at sea level and 40,000 feet is presented in figure 38. It can be seen from this figure that the damping time decreases from $M = 0.75$ to $M = 1.1$ and remains relatively constant to $M = 1.2$, the upper Mach number limit covered by the tests. The period becomes quite short at supersonic speeds as shown in figure 39, which gives the variation of period with Mach number for sea level and 40,000 feet.

CONCLUSIONS

From flight tests at transonic and supersonic speeds of rocket-propelled models of an airplane configuration incorporating a sweptback wing with inverse taper the following conclusions are indicated:

Aerodynamic Parameters

1. The models tested with the conventional tail arrangement gave a higher value of minimum drag coefficient $C_{D_{min}}$ than the models tested with the V-tail arrangement throughout the Mach number range from $M = 0.70$ to $M = 1.15$. The value of $C_{D_{min}}$ obtained from the models with a conventional tail assembly was relatively constant at 0.0195 from a Mach number of 0.60 to $M = 0.85$ increasing to approximately 0.060 at $M = 1.0$ with a gradual increase to a value of 0.065 at $M = 1.15$.

2. No large or abrupt changes occurred in lift-curve slope between $M = 0.62$ and $M = 1.18$, although there is evidence of nonlinearity between positive and negative lift coefficients throughout the speed range covered by the tests.

3. Buffeting was obtained in abrupt pull-ups at high lift coefficients from $M = 0.43$ to $M = 0.78$. The maximum lift coefficient obtained was about 0.75.

4. The hinge-moment coefficient per degree of elevator deflection showed an increase from a value of -0.007 at $M = 0.9$ to -0.017 at $M = 1.10$ and then a gradual decrease to $M = 1.2$.

5. The elevator effectiveness in producing pitching moment was reduced by about 60 percent from $M = 0.70$ to $M = 1.18$.

6. The aerodynamic-center location varied with lift coefficient between $M = 0.75$ and $M = 1.0$. The most-forward aerodynamic-center location of 23 percent of the mean aerodynamic chord occurred at $M = 0.8$ and the most-rearward location of 52 percent occurred at $M = 1.2$.

7. The damping parameters and coefficients indicated that the configuration possessed dynamic longitudinal stability throughout the test speed range.

Flying Qualities

1. The transonic trim change, a pitching-up tendency, is mild.

2. The rates of change of elevator angle required for level flight through the transonic region are sufficiently low at both sea level and 40,000 feet so that a pilot would experience no difficulty in maintaining level flight provided the stick forces are satisfactory.

3. The maneuverability of the airplane would be limited in the transonic speed range at high altitudes as a result of large reduction in control effectiveness and at low speeds due to stalling.

4. Stick forces required for maneuvering will be high at transonic and supersonic speeds necessitating some type of control-boost system.

5. The damping of the short-period longitudinal oscillation is adequate at sea level but is reduced at altitude.

Langley Aeronautical Laboratory
National Advisory Committee for Aeronautics
Langley Air Force Base, Va.

REFERENCES

1. Parks, James H., and Mitchell, Jesse L.: Longitudinal Trim and Drag Characteristics of Rocket-Propelled Models Representing Two Airplane Configurations. NACA RM L9L22, 1950.
 2. Alexander, Sidney R.: Flight Investigation to Determine the Aerodynamic Characteristics of Rocket-Powered Models Representative of a Fighter-Type Airplane Configuration Incorporating an Inverse-Taper Wing and a Vee Tail. NACA RM L8G29, 1948.
 3. Strass, H. Kurt, Fields, E. M., and Schult, E. D.: Free-Flight Investigation at Transonic and Supersonic Speeds of the Rolling Effectiveness of a Partial-Span Aileron on an Inversely Tapered Sweptback Wing. NACA RM L50B08, 1950.
 4. Mitchell, Jesse L., and Peck, Robert F.: An NACA Vane-Type Angle-of-Attack Indicator for Use at Subsonic and Supersonic Speeds. NACA RM L9F28a, 1949.
 5. Mitcham, Grady L., Stevens, Joseph E., and Norris, Harry P.: Aerodynamic Characteristics and Flying Qualities of a Tailless Triangular-Wing Airplane Configuration As Obtained from Flights of Rocket-Propelled Models at Transonic and Low Supersonic Speeds. NACA RM L9L07, 1950.
 6. Gillis, Clarence L., Peck, Robert F., and Vitale, A. James: Preliminary Results from a Free-Flight Investigation at Transonic and Supersonic Speeds of the Longitudinal Stability and Control Characteristics of an Airplane Configuration with a Thin Straight Wing of Aspect Ratio 3. NACA RM L9K25a, 1950.
 7. Mayer, John P.: Effect of Mach Number on the Maximum Lift and Buffeting Boundary Determined in Flight on a North American P-51D Airplane. NACA RM L6I10, 1947.
 8. Purser, Paul E.: Effect of a Pilot's Canopy on the Drag of an NACA RM-2 Drag Research Model in Flight at Transonic and Supersonic Speeds. NACA RM L7L22, 1948.
 9. Alexander, Sidney R.: Effect of Windshield Shape of a Pilot's Canopy on the Drag of an NACA RM-2 Drag Research Model in Flight at Transonic Speeds. NACA RM L8E04, 1948.
 10. Anon.: Flying Qualities of Piloted Airplanes. U. S. Air Force Specification No. 1815-B, June 1, 1948.
- ~~CONFIDENTIAL~~

TABLE I
 GEOMETRIC CHARACTERISTICS OF THE FULL-SCALE AIRPLANE AND THE MODELS

	Full-scale	Models 1 and 2	Models B and C	Model D
Wing:				
Thickness (in free stream), percent	7.6	7.6	7.6	7.6
Incidence, deg	Variable	0	0	0
Twist, deg	0	0	0	0
Sweepback at 0.50c, deg	40	40	40	40
Inverse taper ratio	1:1.626	1:1.626	1:1.626	1:1.626
A	3.07	3.07	3.07	3.07
c̄, ft	10.60	1.590	1.175	1.175
b, ft	31.34	4.70	3.48	3.48
S, sq ft	320.0	7.20	3.95	3.95
Dihedral, deg	-5	-5	0	0
Horizontal tail:				
Section	Symmetrical	Symmetrical		Symmetrical
Thickness (in free stream), percent	7.6	7.6		7.6
Sweepback, deg	40	40		40
b _t , ft	16.68	2.50		1.85
c̄ _t , ft	4.28	0.643		0.476
S _t , sq ft	69.61	1.57		0.86
S _e , sq ft	21.10	0.475		0.26
Incidence, deg	0	0		0
Vertical tail:				
Total area, sq ft	48.30	1.085		0.593
V-tail:				
Section			Symmetrical	
Thickness (in free stream), percent			7.6	
Sweepback, plan view, deg			40	
Dihedral, deg			38	
b _t , plan view, ft			1.81	
c̄ _t , ft			0.437	
S _t , plan view, sq ft			0.935	
S _t , side view, sq ft			0.730	
S _t , actual, sq ft			1.187	
Incidence, deg			0	

NACA

TABLE II
WEIGHT AND BALANCE DATA

	Weight (lb)	Wing loading (lb/sq ft)	Moments of inertia in pitch, I_Y (slug-ft ²)	Center-of-gravity location (percent M.A.C.)
Full-scale airplane	18,600	58.2	48,724	18.0
Model 1	162.75	22.60	17.03	5.6
Model 2	158.0	21.90	15.34	12.5
Model B	40.8	10.32	-----	-4.0
Model C	37.8	9.60	2.06	4.5
Model D	37.7	9.58	2.23	8.50

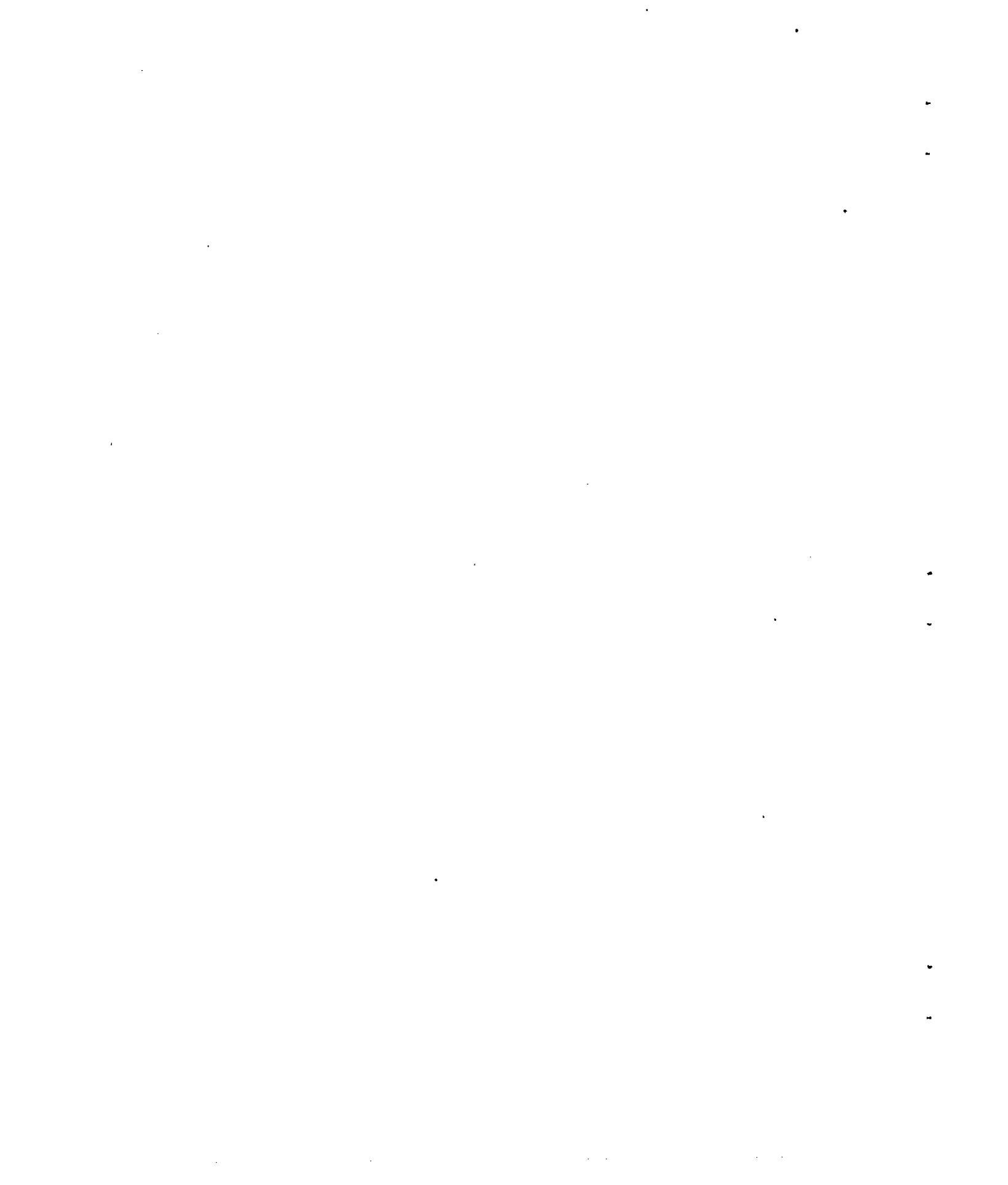


TABLE III

WING AIRFOIL ORDINATES PARALLEL TO AIRPLANE CENTER LINE

Station (percent chord)	Upper (percent chord)		Lower (percent chord)	
	Root section	Tip section	Root section	Tip section
0.5	0.63	0.66	0.51	0.54
.75	.78	.81	.64	.67
1.25	1.01	1.05	.82	.86
2.50	1.44	1.48	1.15	1.19
5.00	2.05	2.09	1.60	1.63
7.50	2.52	2.53	1.92	1.94
10.00	2.88	2.89	2.17	2.18
15	3.44	3.44	2.53	2.53
20	3.84	3.84	2.78	2.78
25	4.13	4.13	2.94	2.94
30	4.32	4.32	3.04	3.04
35	4.44	4.44	3.08	3.08
40	4.48	4.48	3.08	3.08
45	4.45	4.45	3.01	3.01
50	4.36	4.36	2.89	2.89
55	4.15	4.15	2.72	2.72
60	3.89	3.89	2.50	2.50
65	3.57	3.57	2.23	2.23
70	3.19	3.19	1.93	1.93
75	2.75	2.75	1.60	1.60
80	2.27	2.27	1.25	1.25
85	1.75	1.75	.89	.89
90	1.21	1.21	.54	.54
95	.63	.63	.24	.24
100	0	0	0	0

NACA



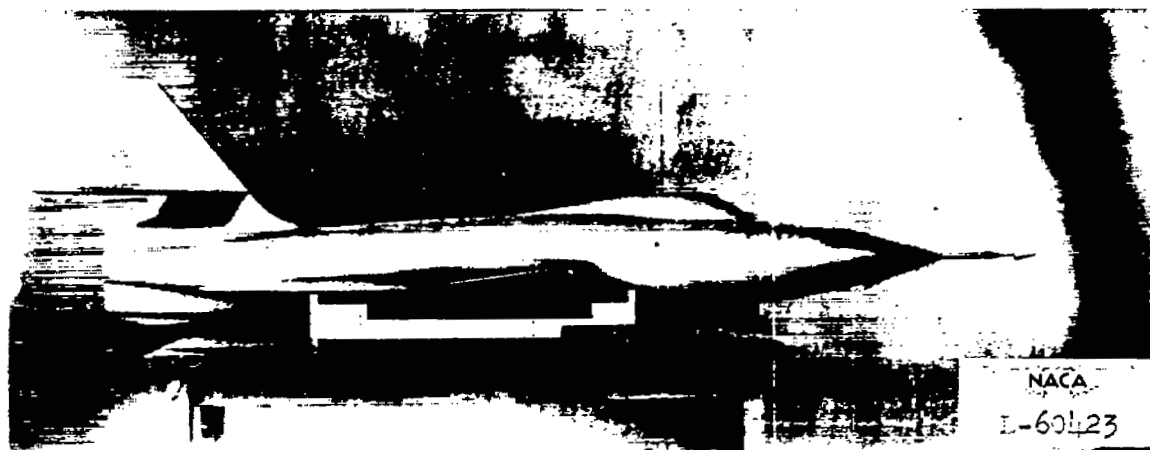
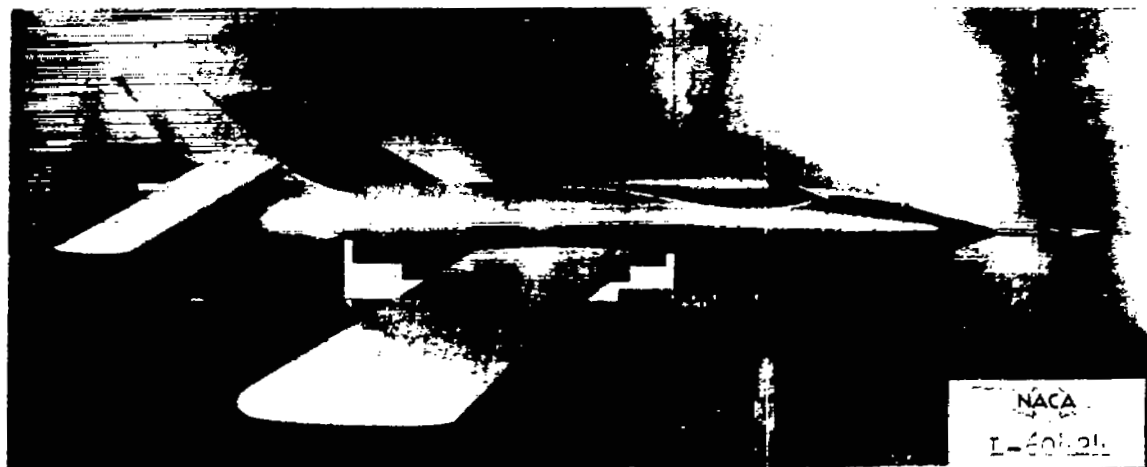


Figure 2.- Two views of one of the pulsed models.

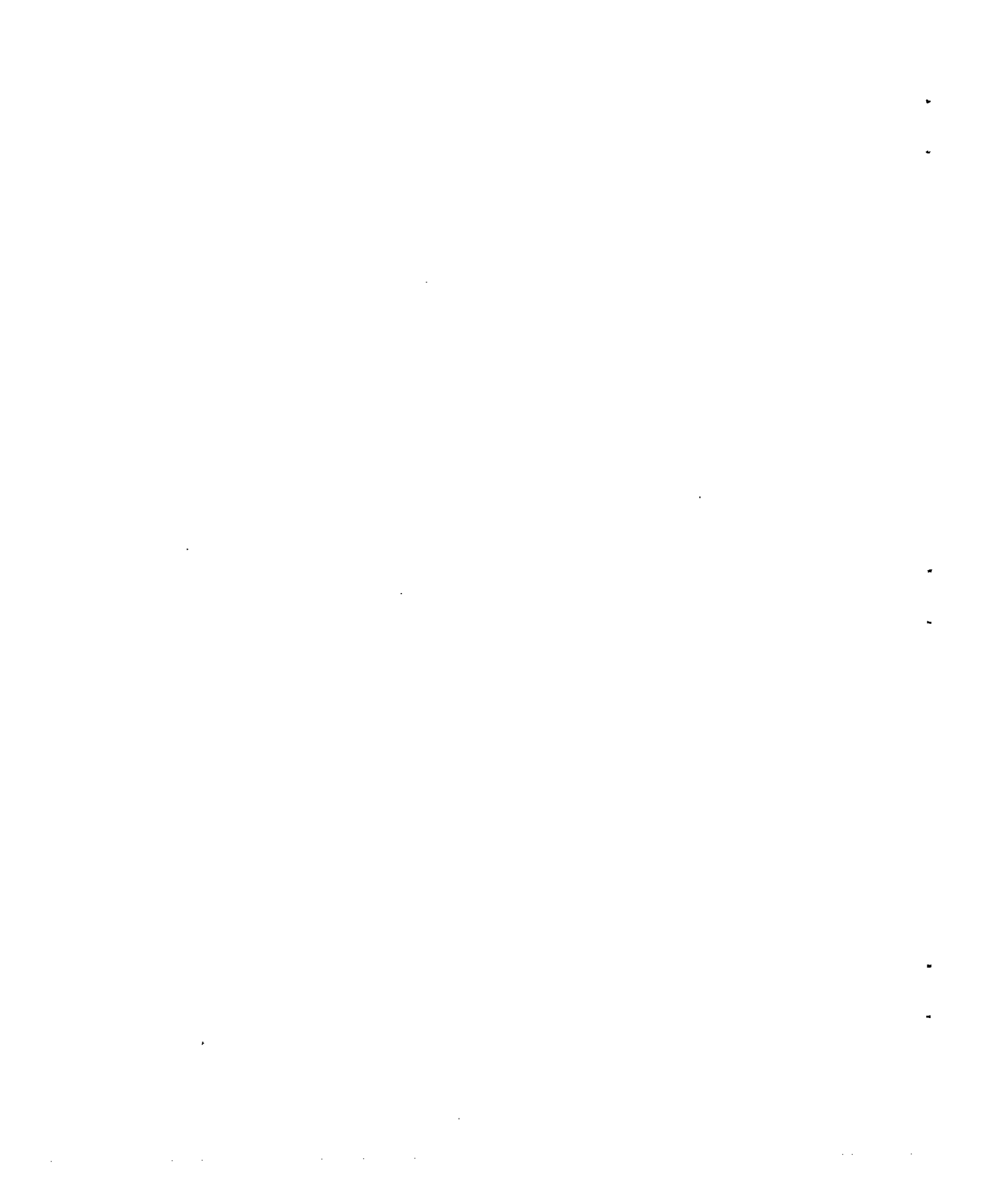




Figure 3.- One of the pulsed T-tail models in launching position.



A



Figure 4.- Photographs of launching of one of the pulsed models.


L-64894



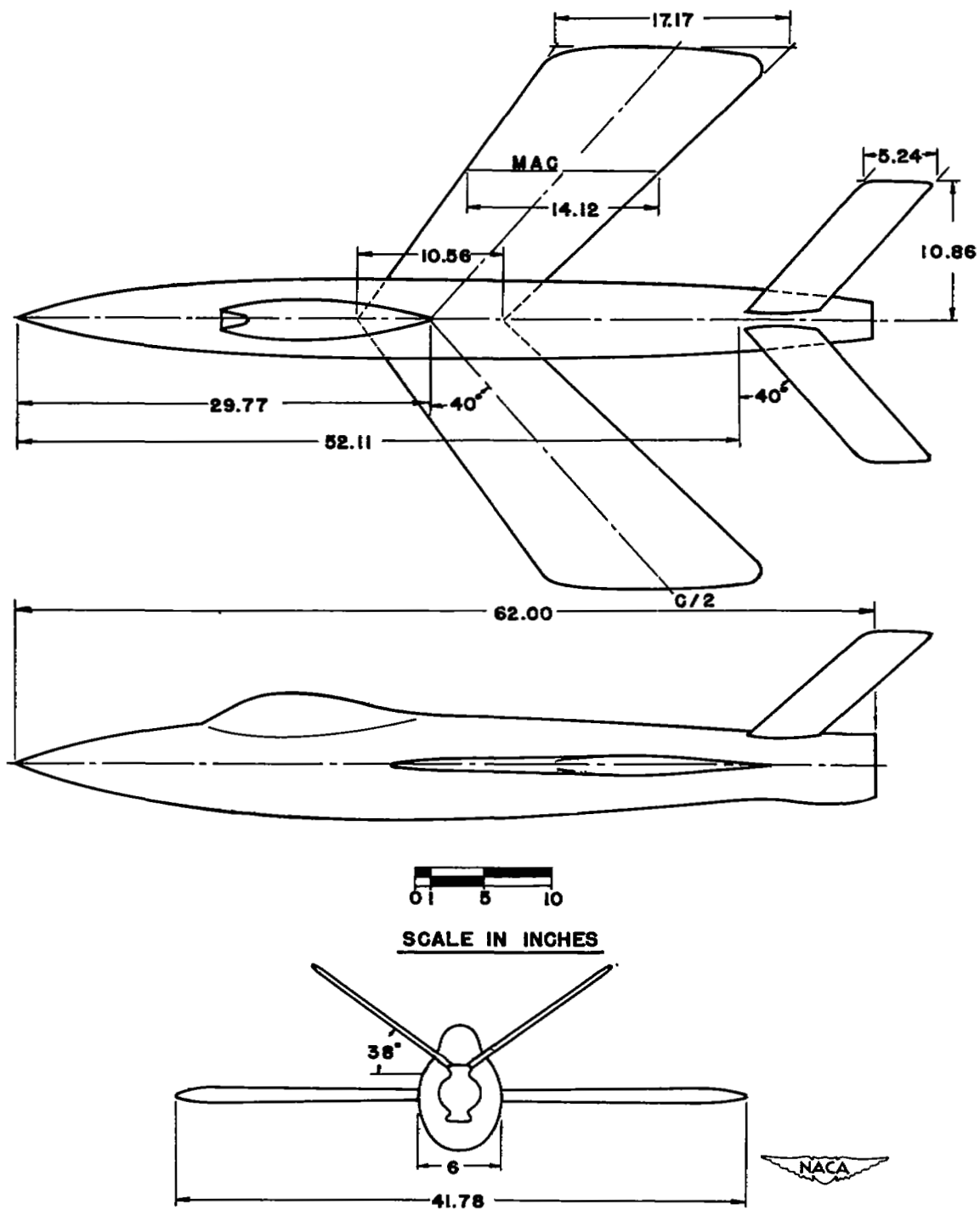
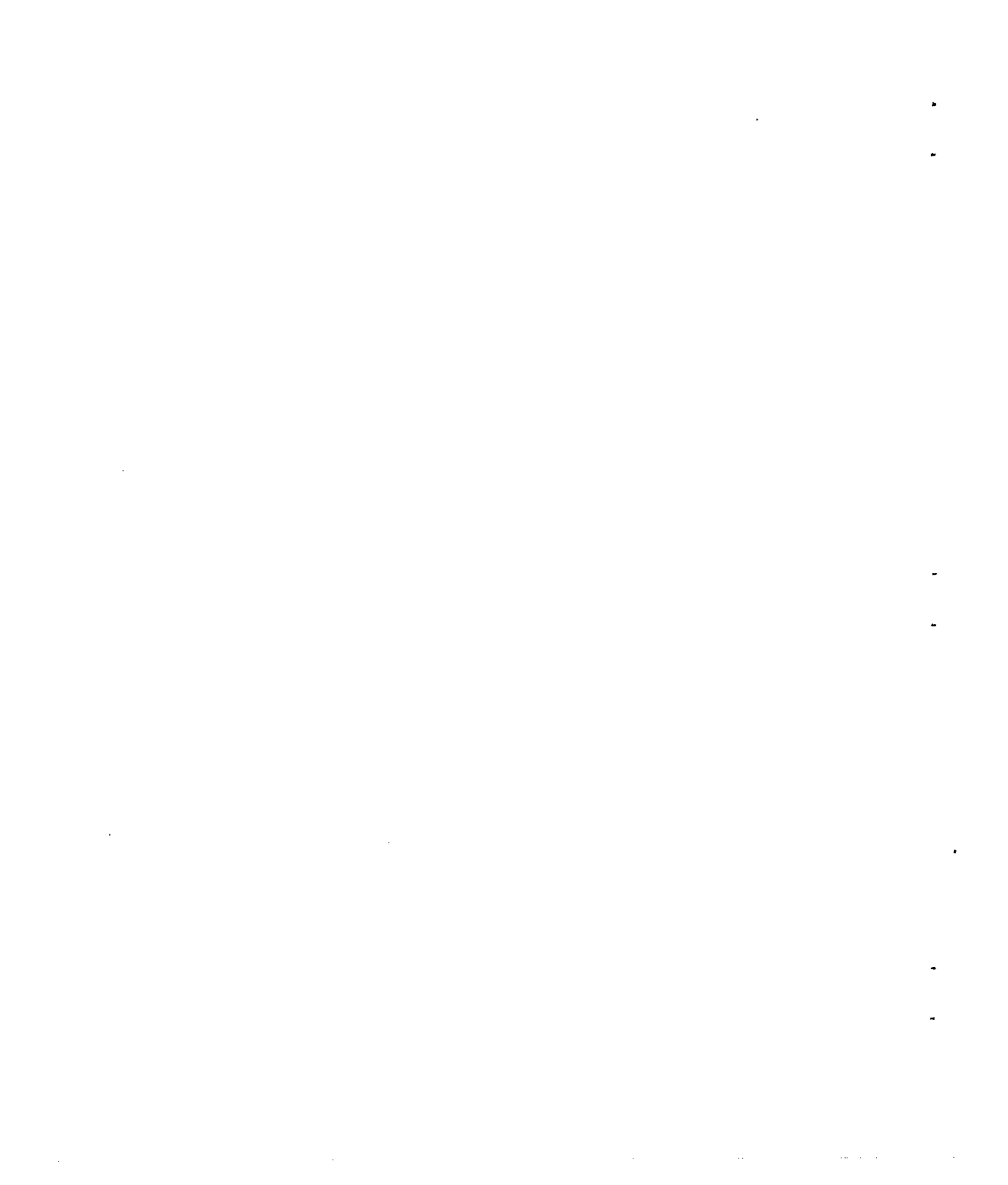


Figure 5.- Three-view drawing of models B and C.



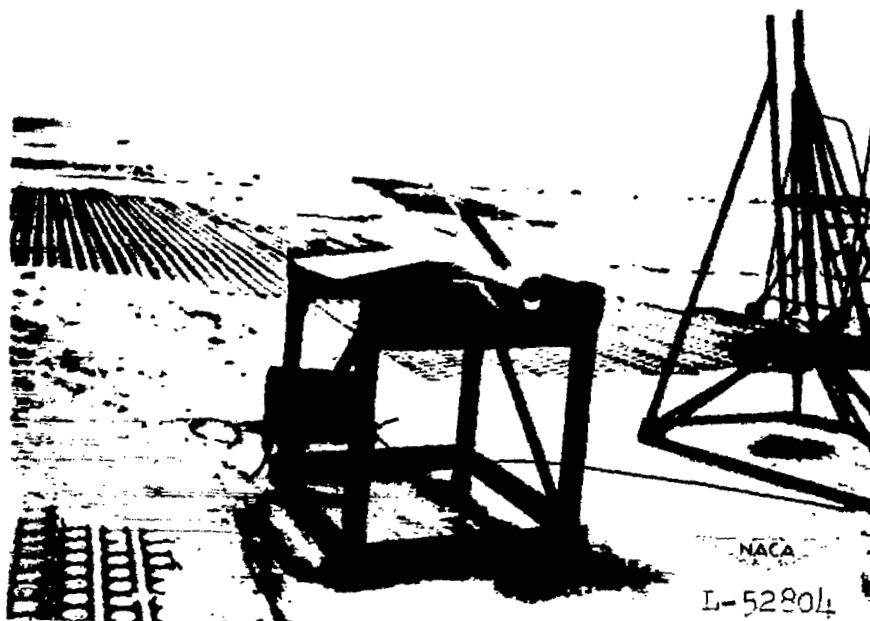
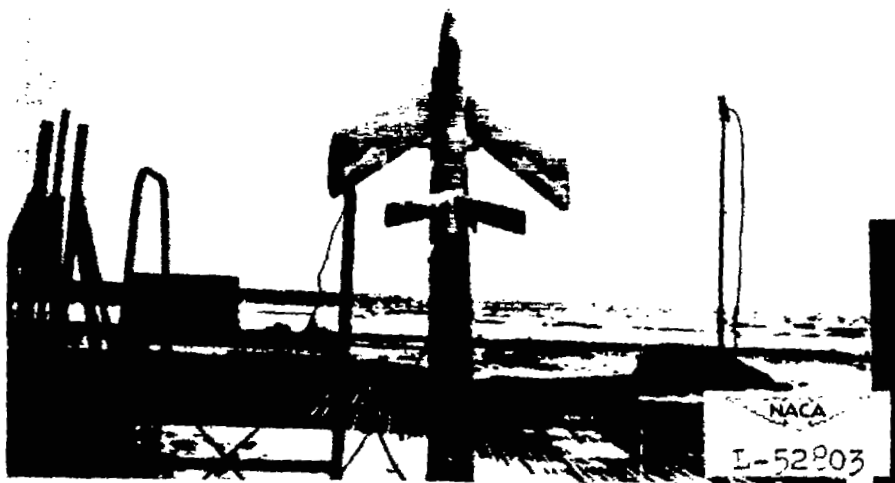
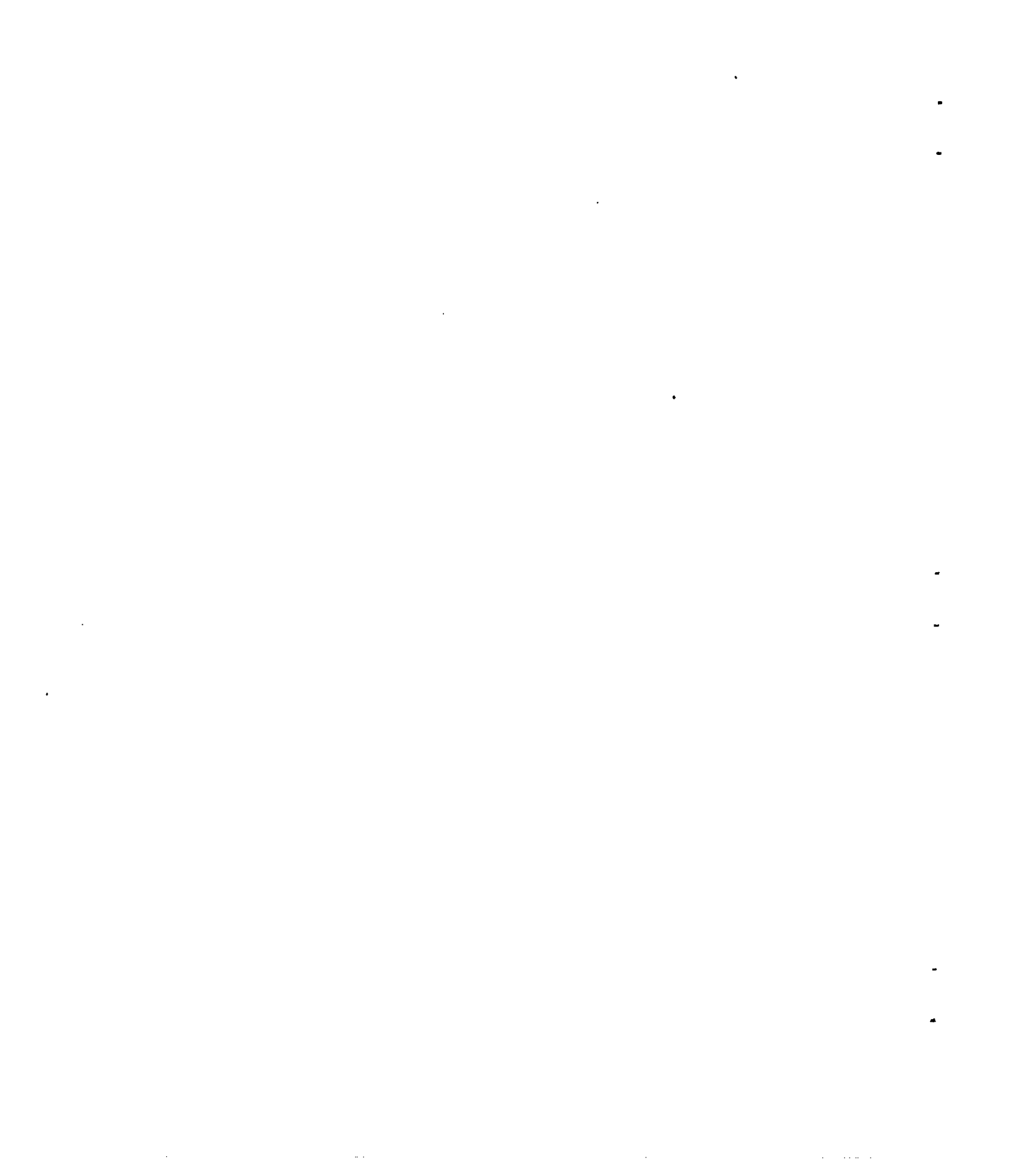


Figure 6.- Two views of one of the fixed-control V-tail models.



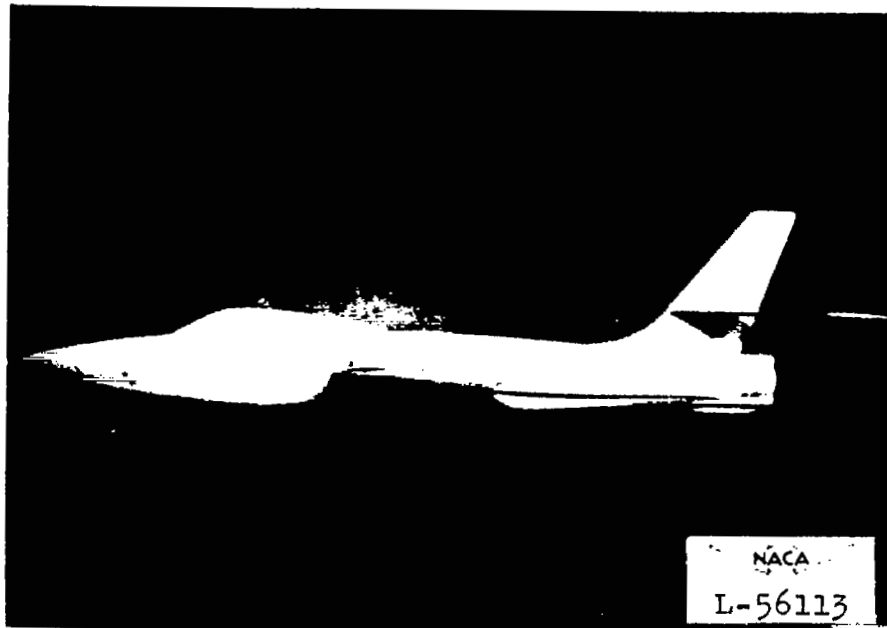
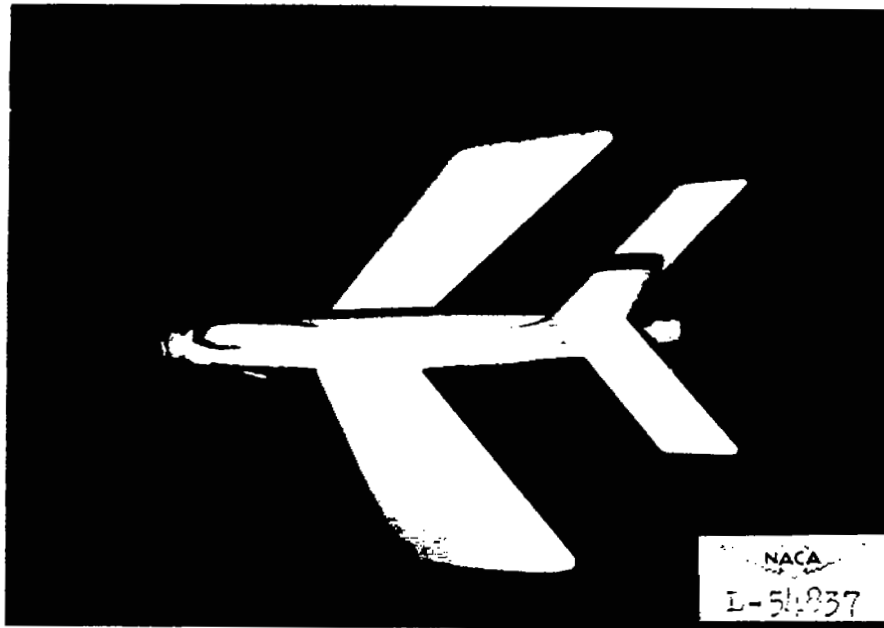


Figure 7.- Two views of the fixed-control T-tail model.



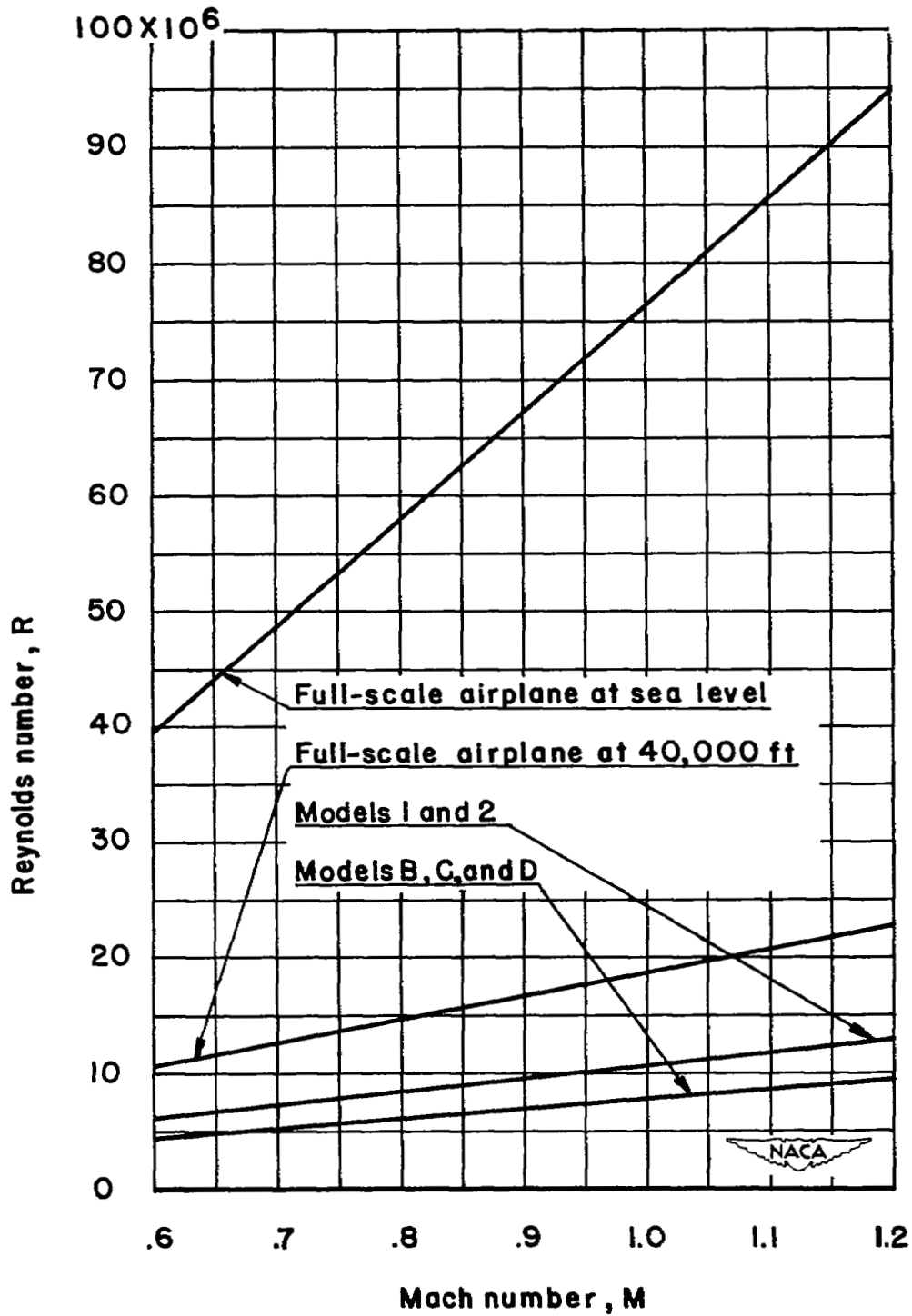


Figure 8.- Variation of Reynolds number with Mach number (based on mean aerodynamic chord).

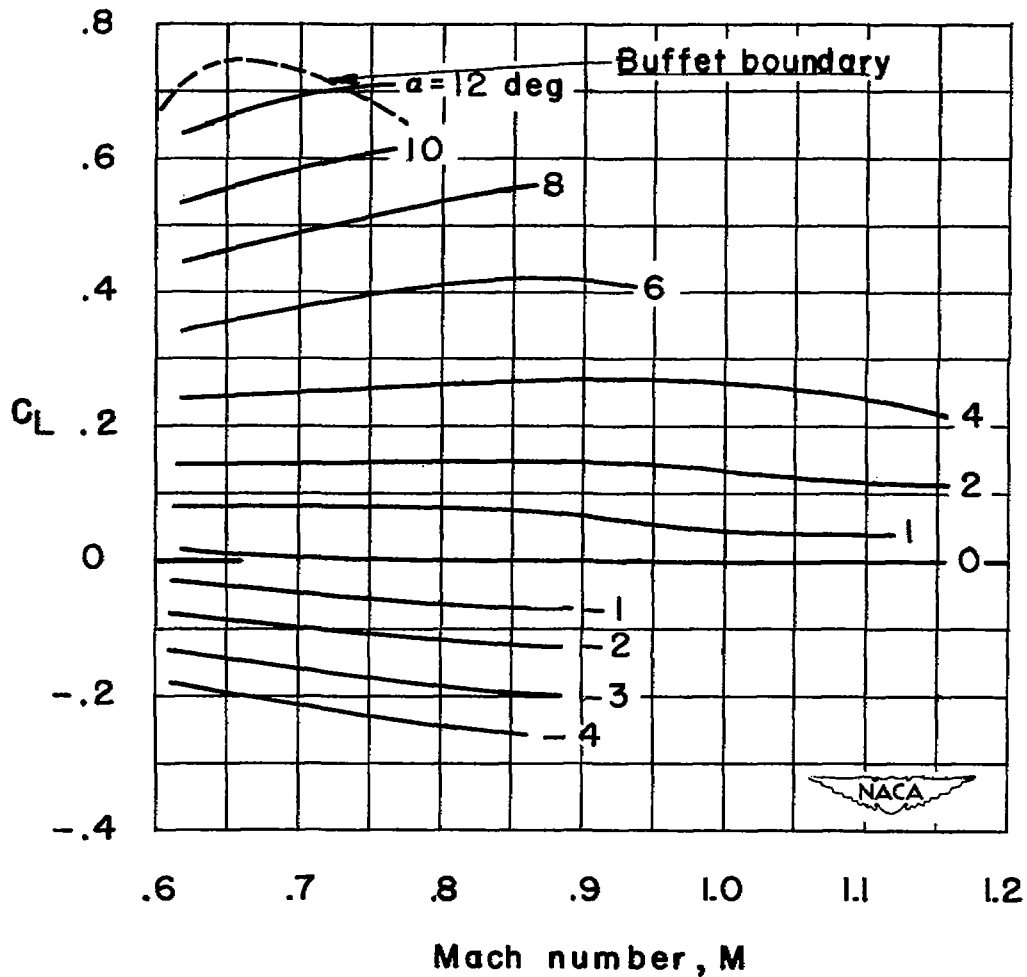
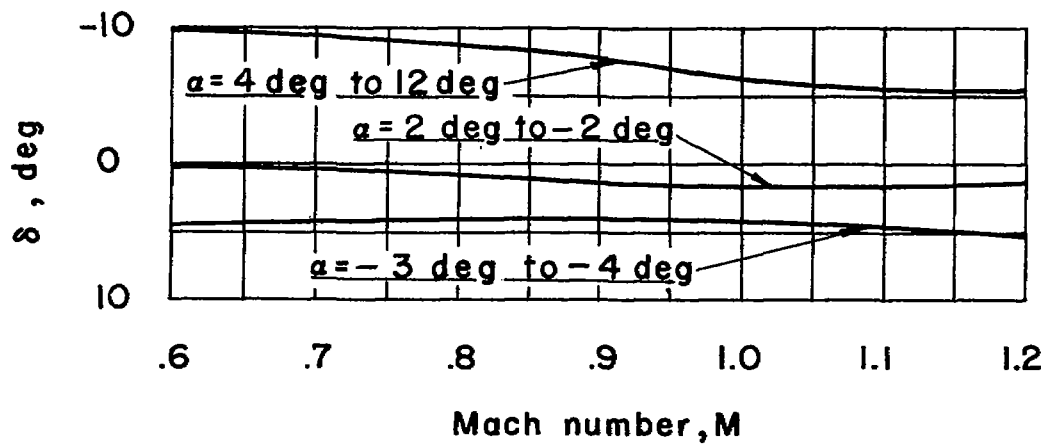


Figure 9.- Lift at constant angle of attack as a function of Mach number.

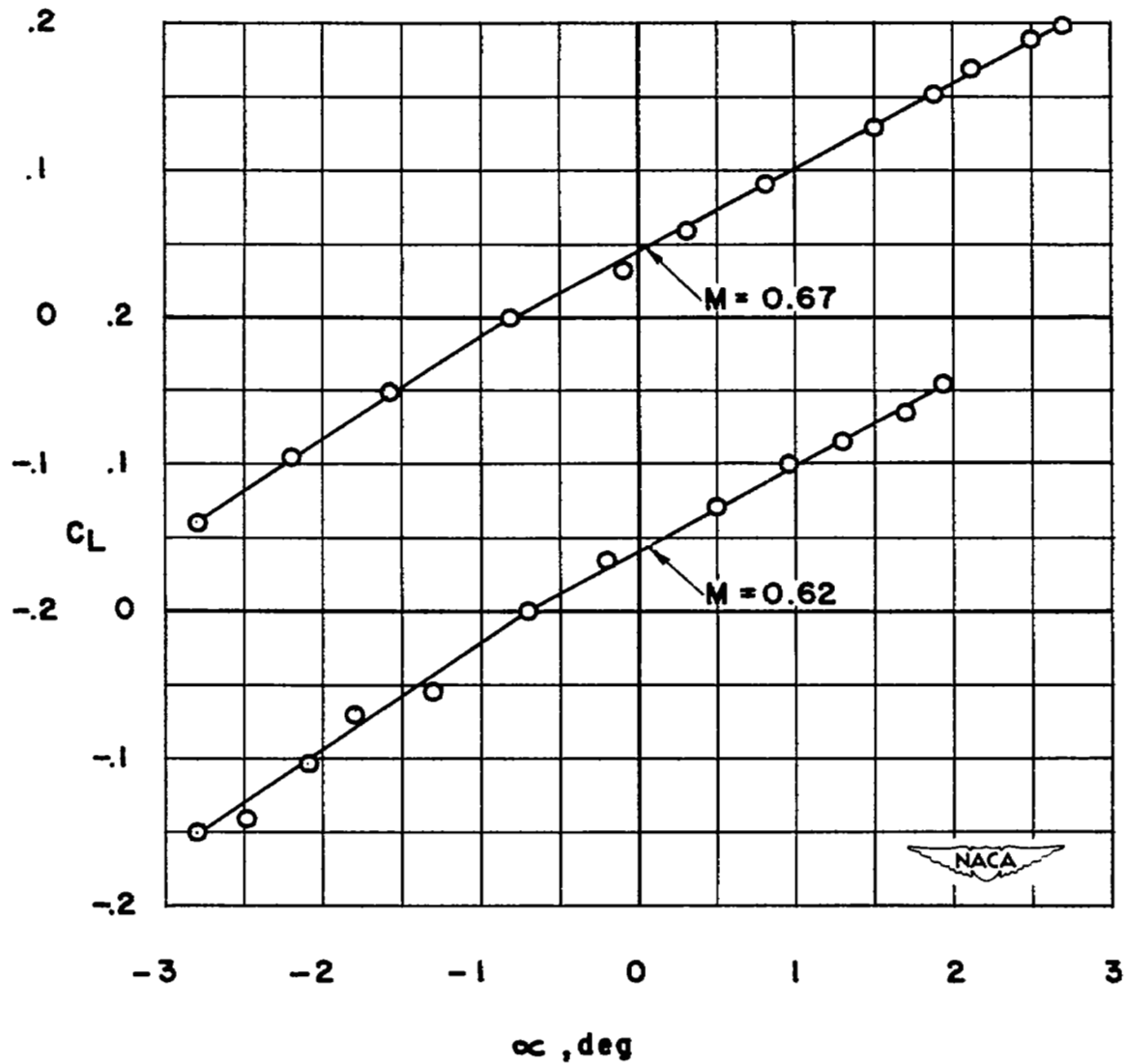


Figure 10.- Variation of lift coefficient with angle of attack, showing nonlinearity near zero lift coefficients, as obtained from model 1.

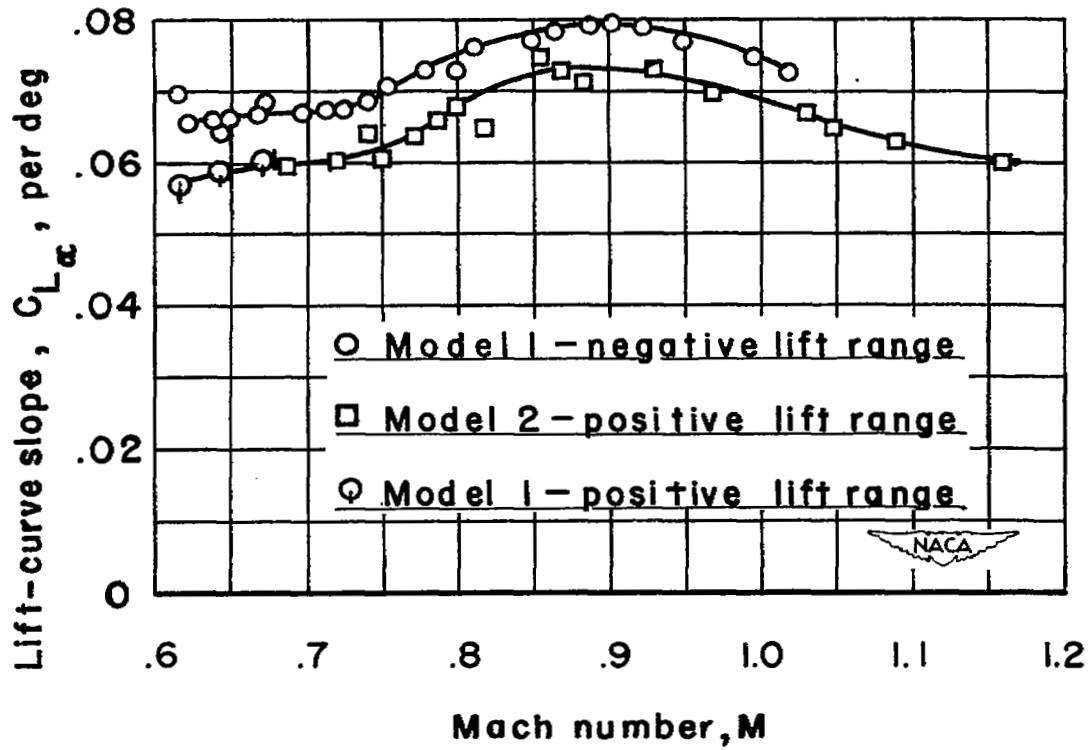


Figure 11.- Variation of lift-curve slope with Mach number.

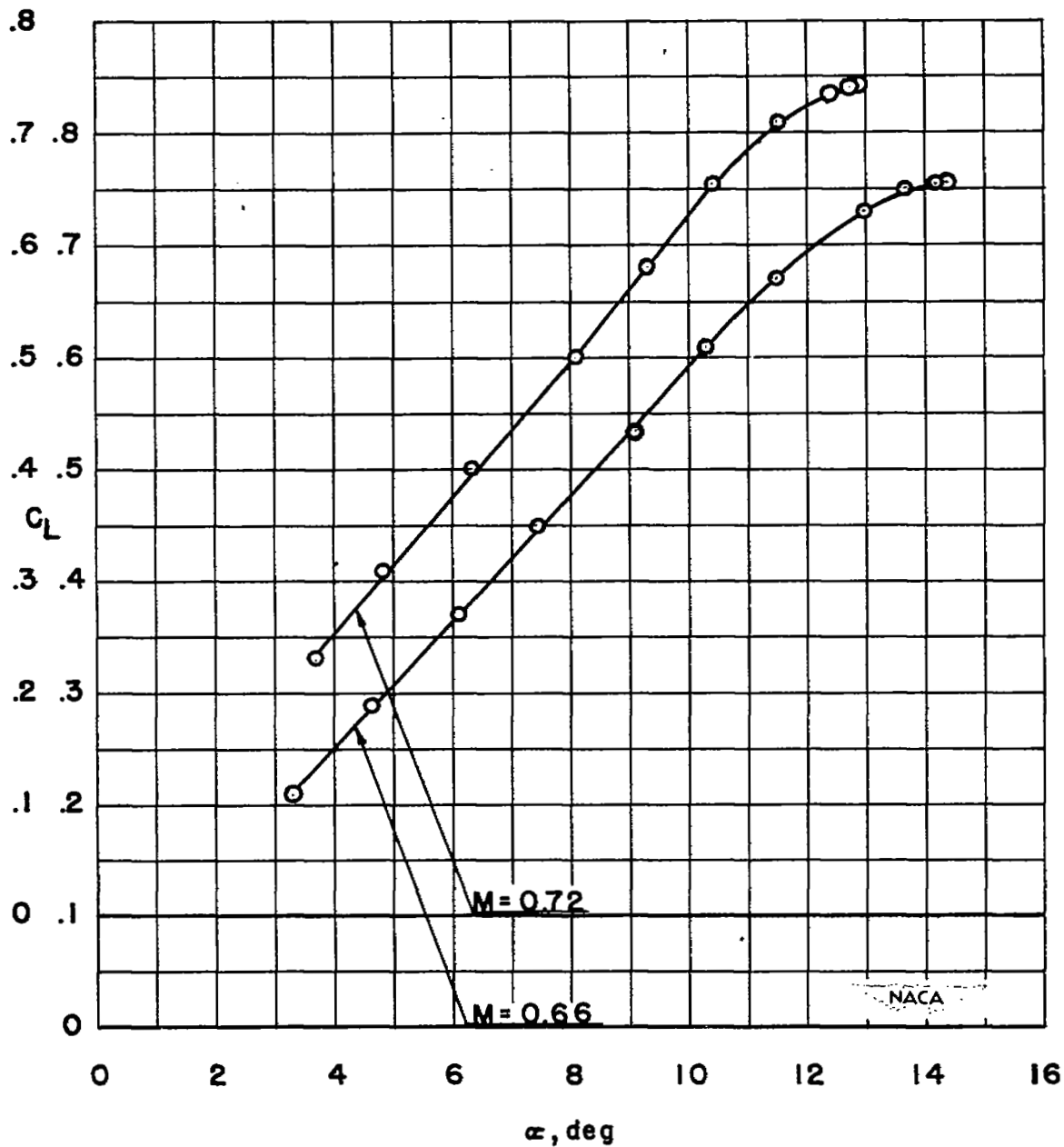


Figure 12.- Variation of lift coefficient with angle of attack, showing the approach to maximum lift as obtained from model 2.

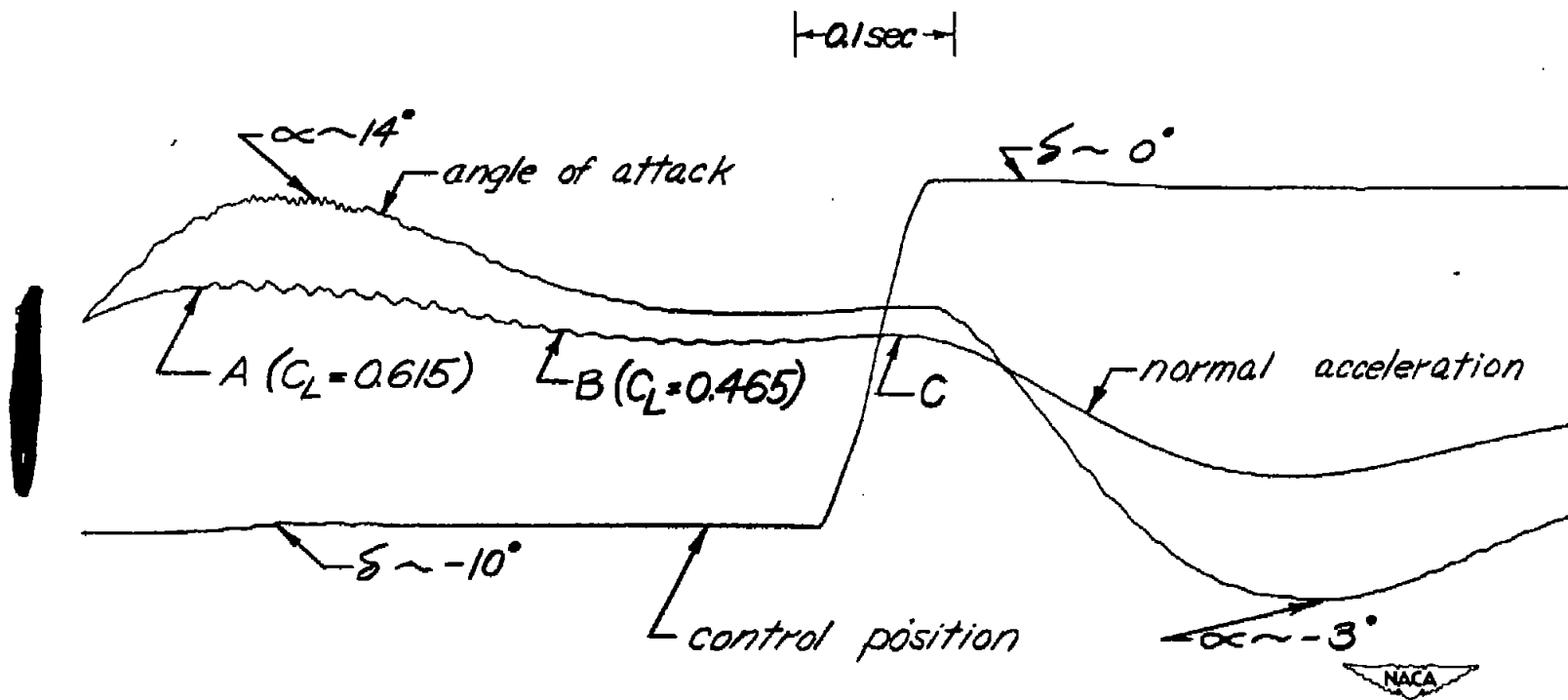


Figure 13.- Section of telemeter record showing buffet oscillation, model 2.

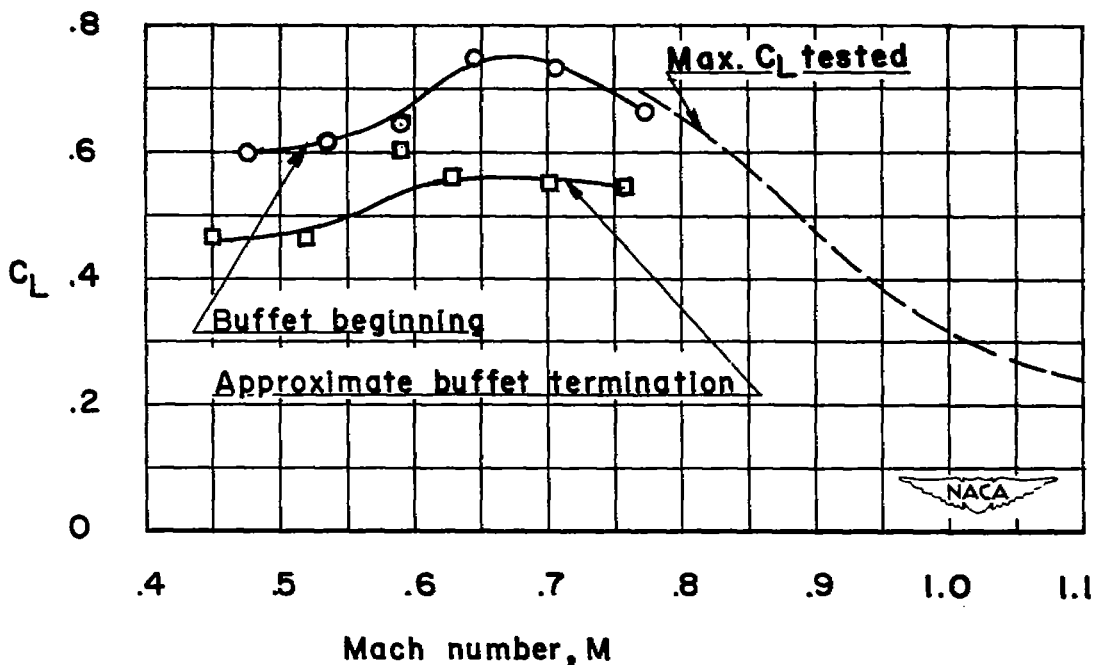


Figure 14.- Variation with Mach number of the buffet boundaries.

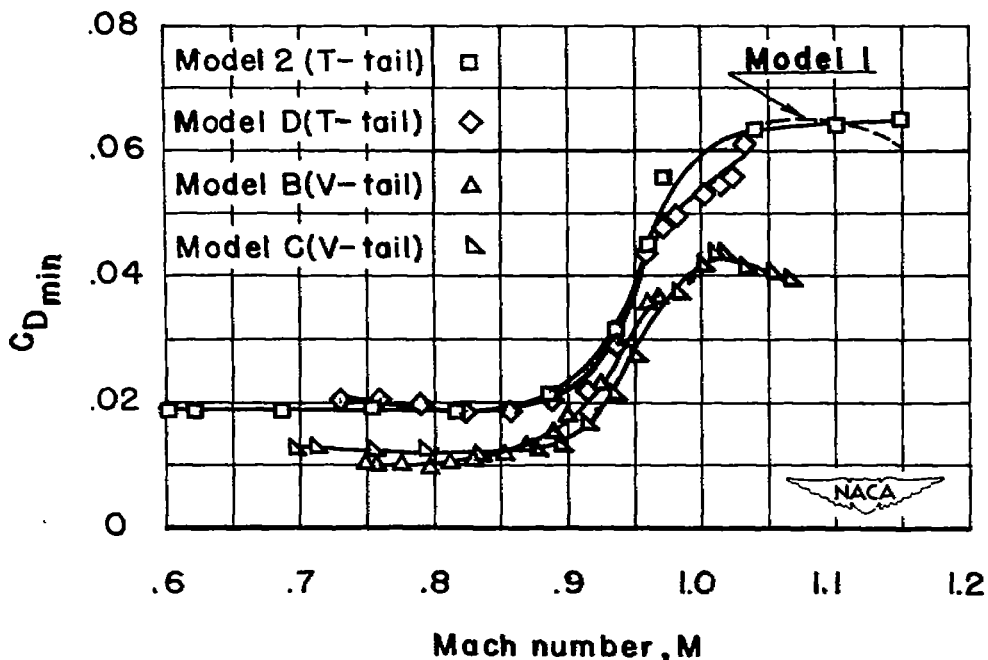


Figure 15.- Variation with Mach number of drag coefficient at approximately zero lift.

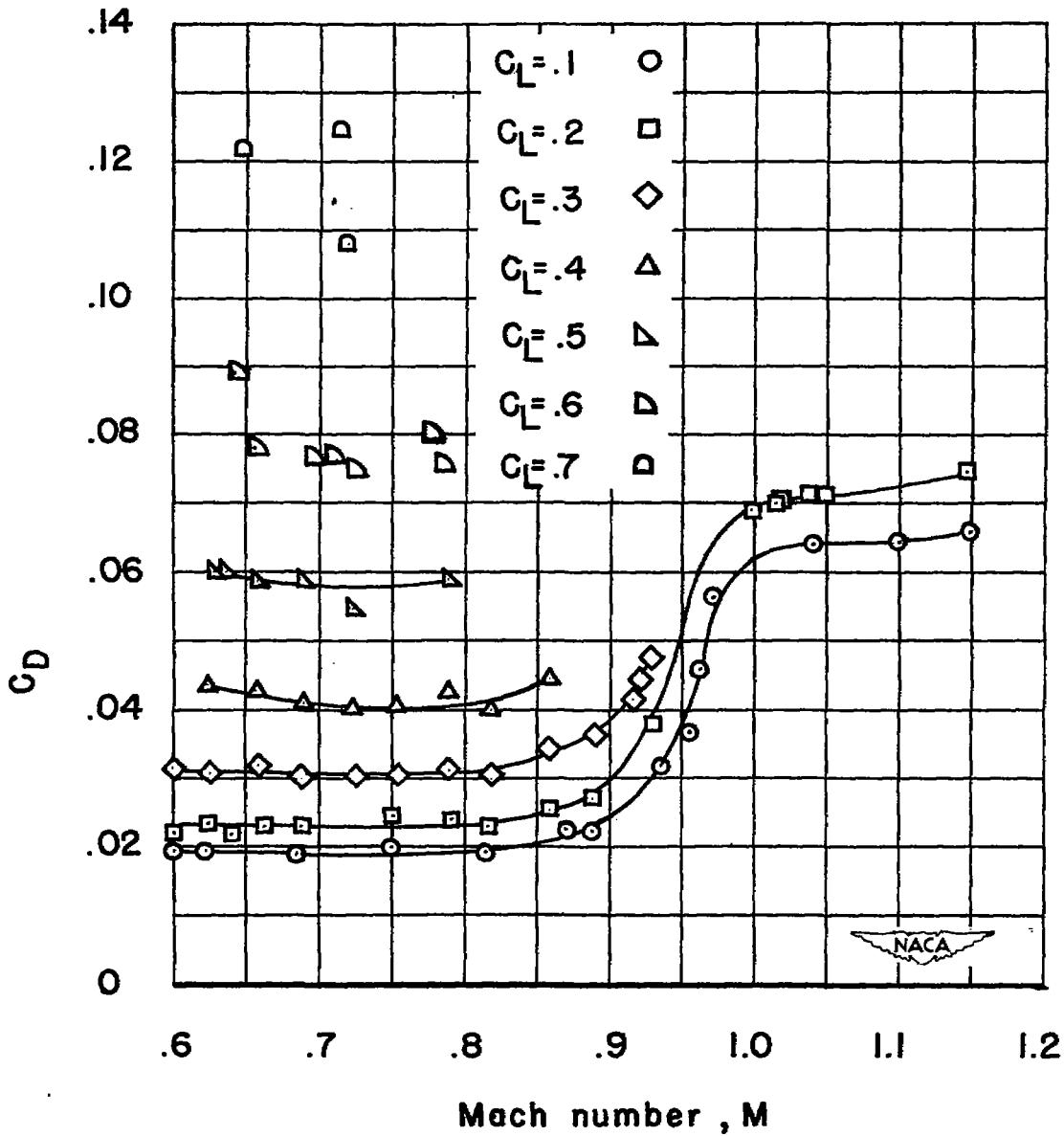


Figure 16.- Variation with Mach number of drag coefficients at various lift coefficients, as obtained from model 2.

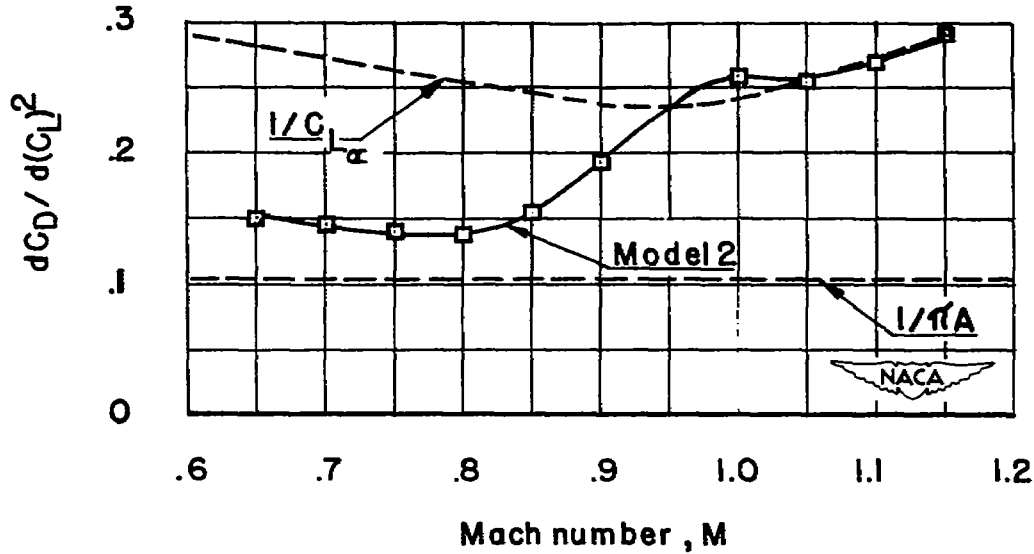


Figure 17.- Variation with Mach number of the effect of lift on drag.

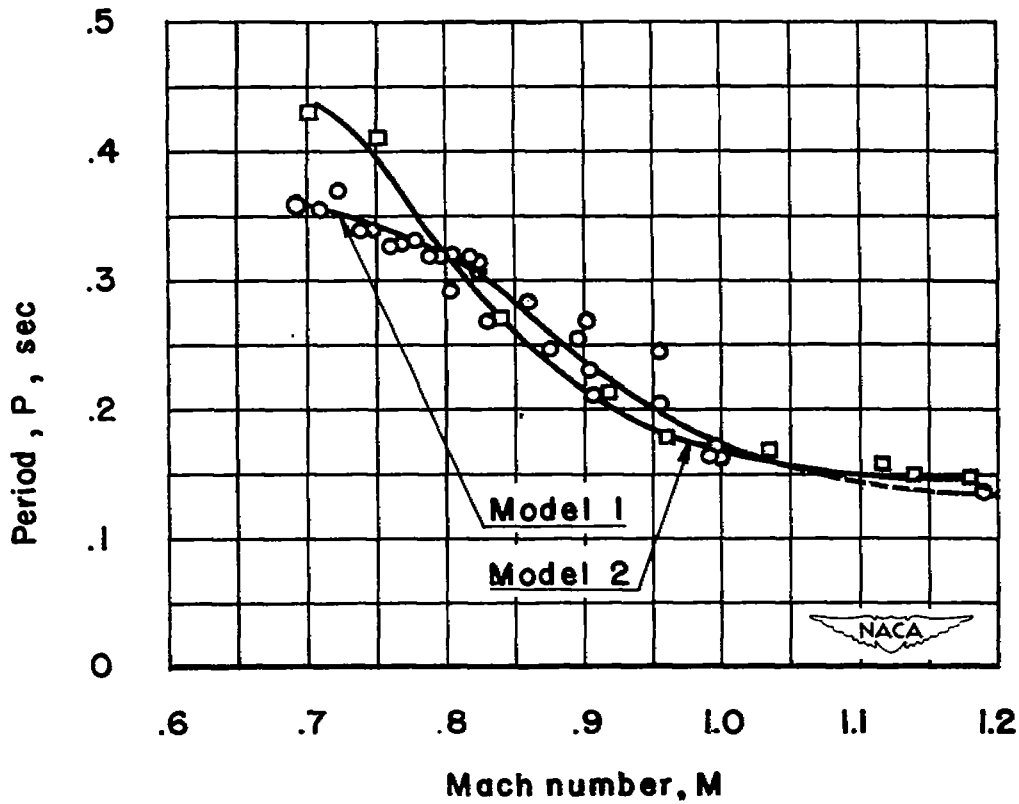


Figure 18.- Period of short-period longitudinal oscillation as a function of Mach number.

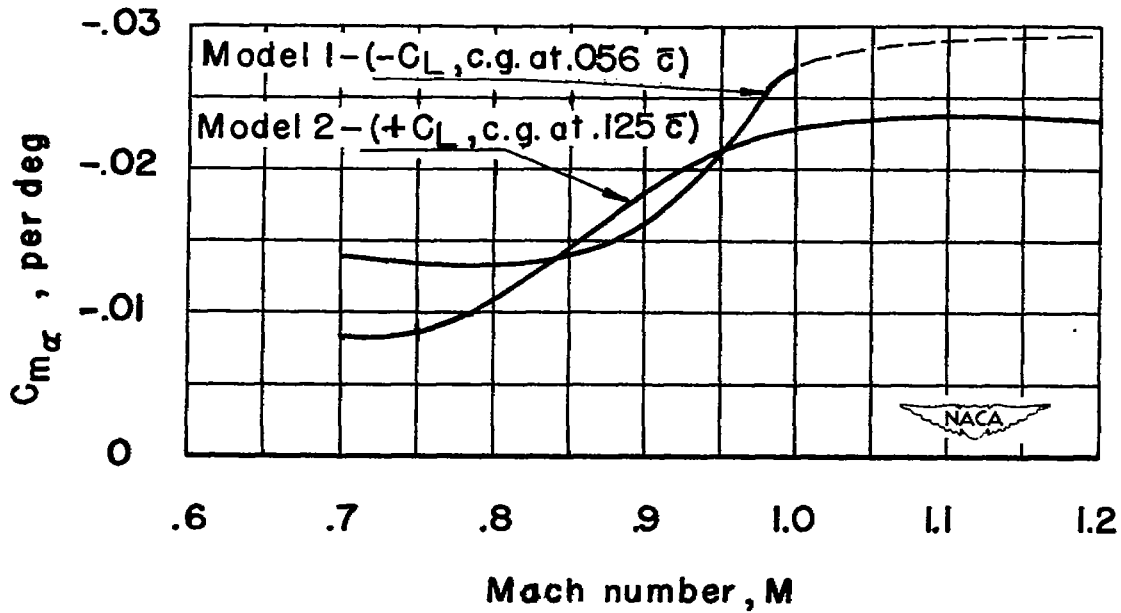


Figure 19.- Rate of change of pitching-moment coefficient with angle of attack as a function of Mach number.

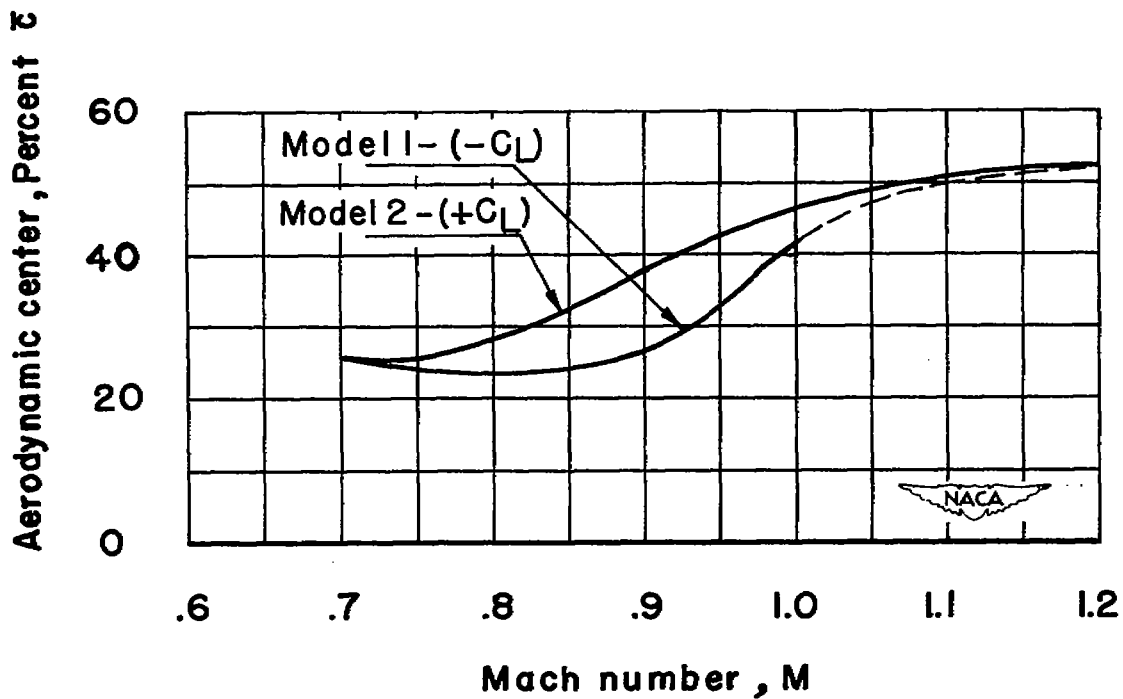


Figure 20.- Variation of aerodynamic-center location with Mach number.

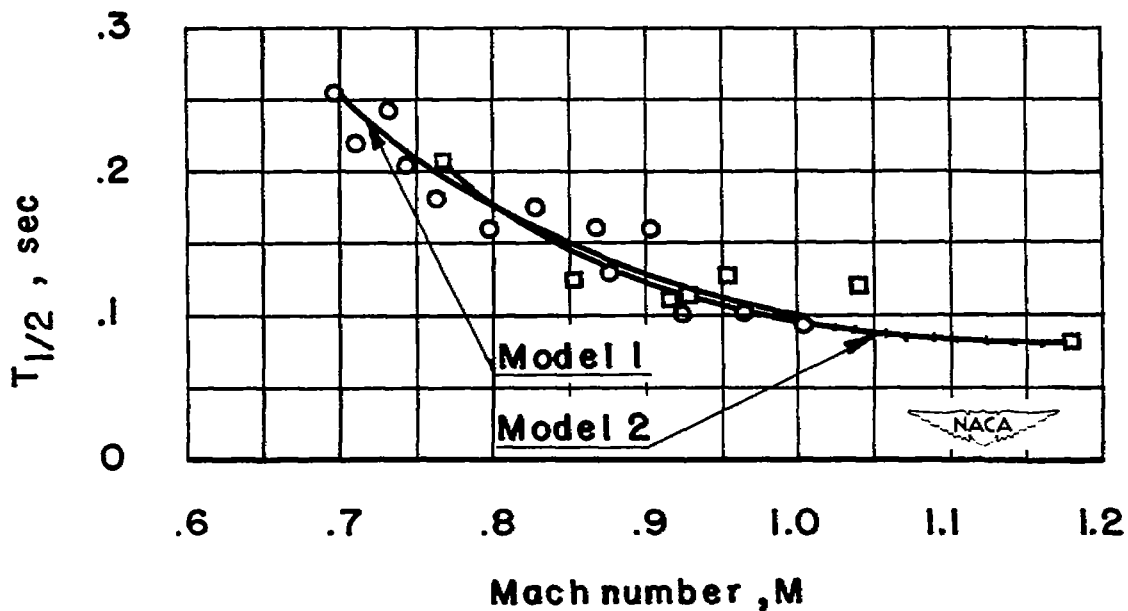


Figure 21.- Time required for short-period longitudinal oscillation to damp to one-half amplitude.

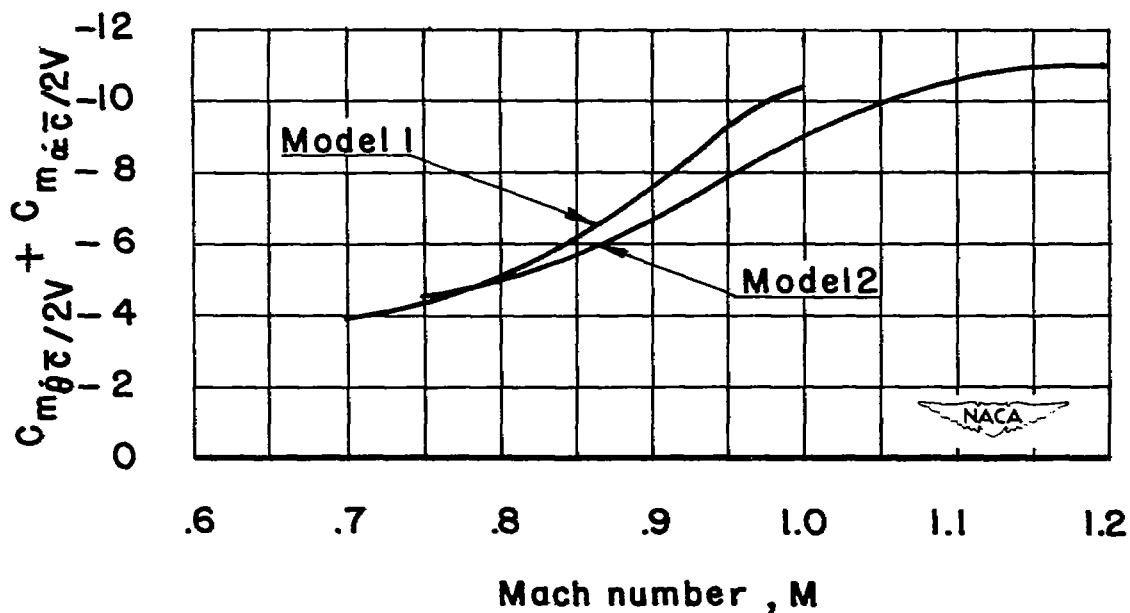


Figure 22.- Variation of total damping coefficient with Mach number.

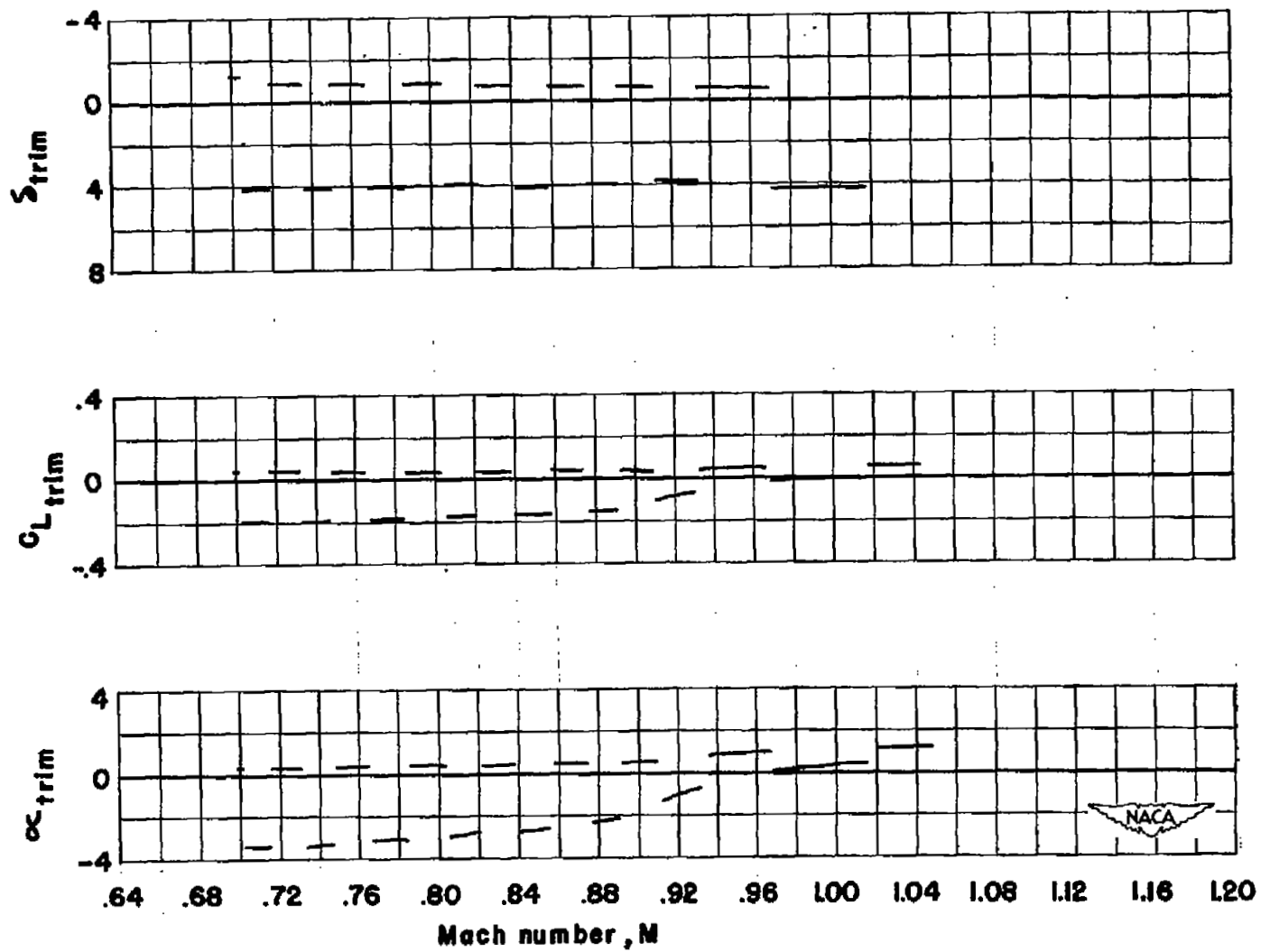


Figure 23.- Variation with Mach number of α_{trim} , $C_{L_{trim}}$, and δ_{trim} for model 1.

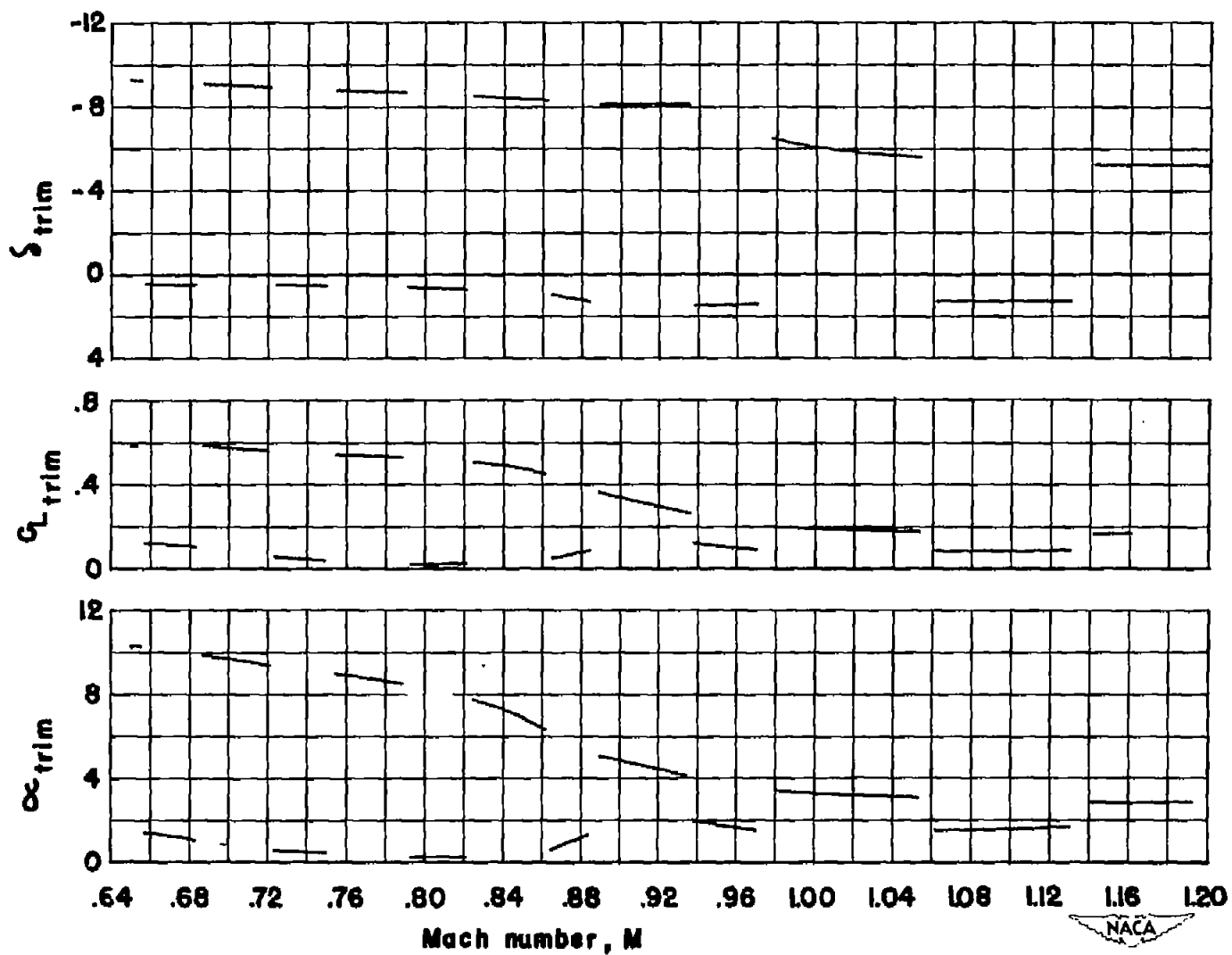


Figure 24.- Variation with Mach number of α_{trim} , $C_{L_{trim}}$, and δ_{trim} for model 2.

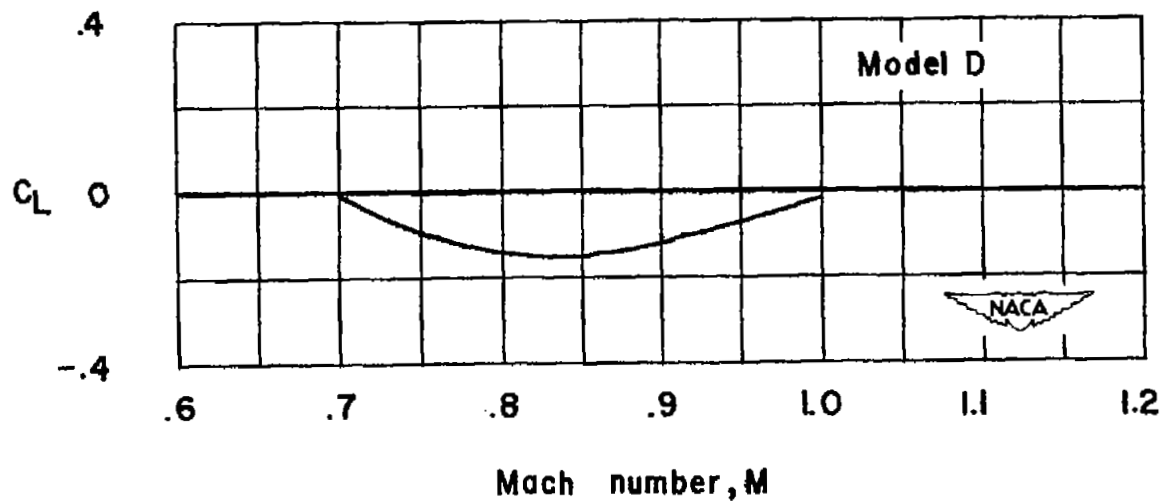
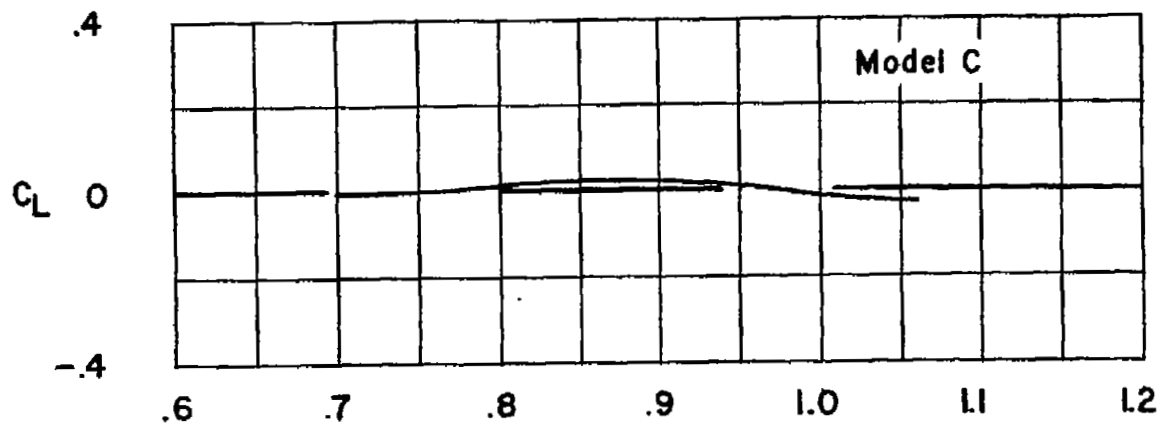


Figure 25.- Variation of longitudinal trim with Mach number for models C and D. $\delta = 0^\circ$.

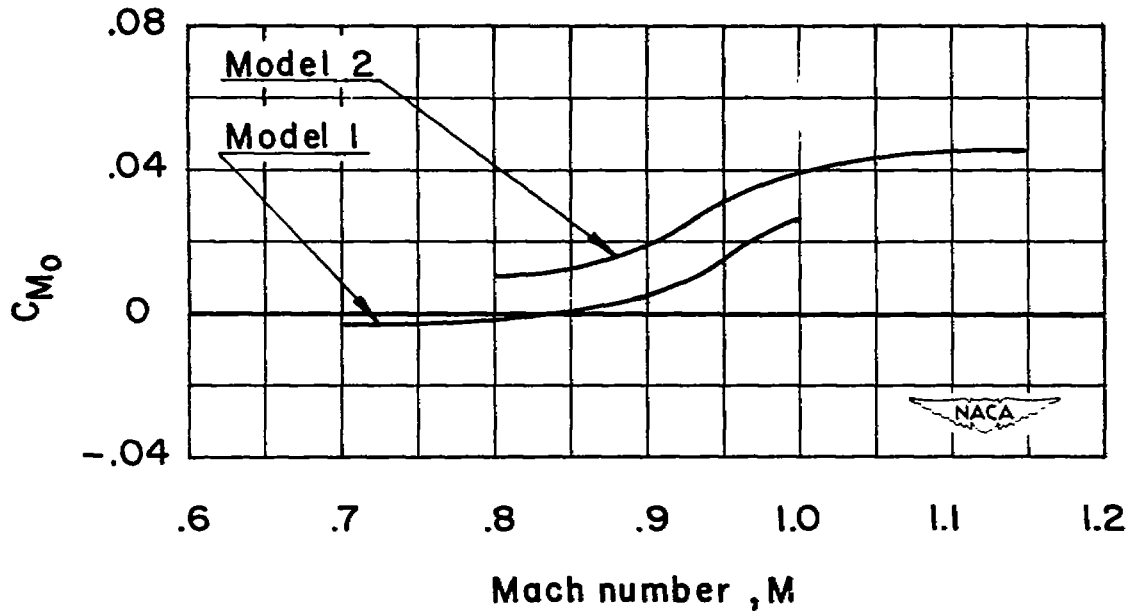


Figure 26.- Variation with Mach number of zero-angle-of-attack pitching-moment coefficient for zero stabilizer incidence.

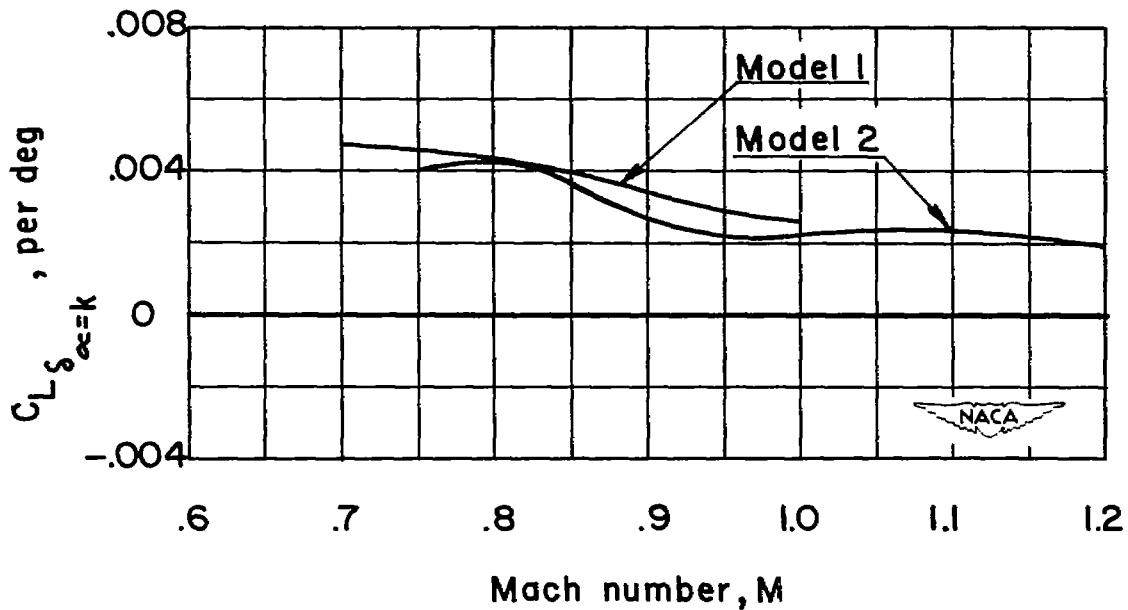


Figure 27.- Variation with Mach number of rate of change of lift coefficient with respect to elevator deflection at constant angle of attack.

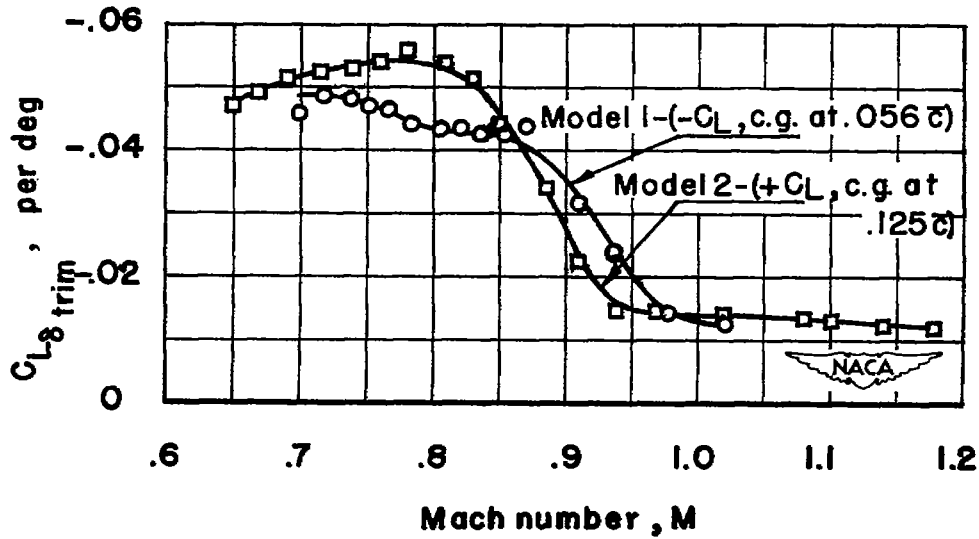


Figure 28.- Variation with Mach number of the rate of change of trim lift coefficient with respect to elevator deflection

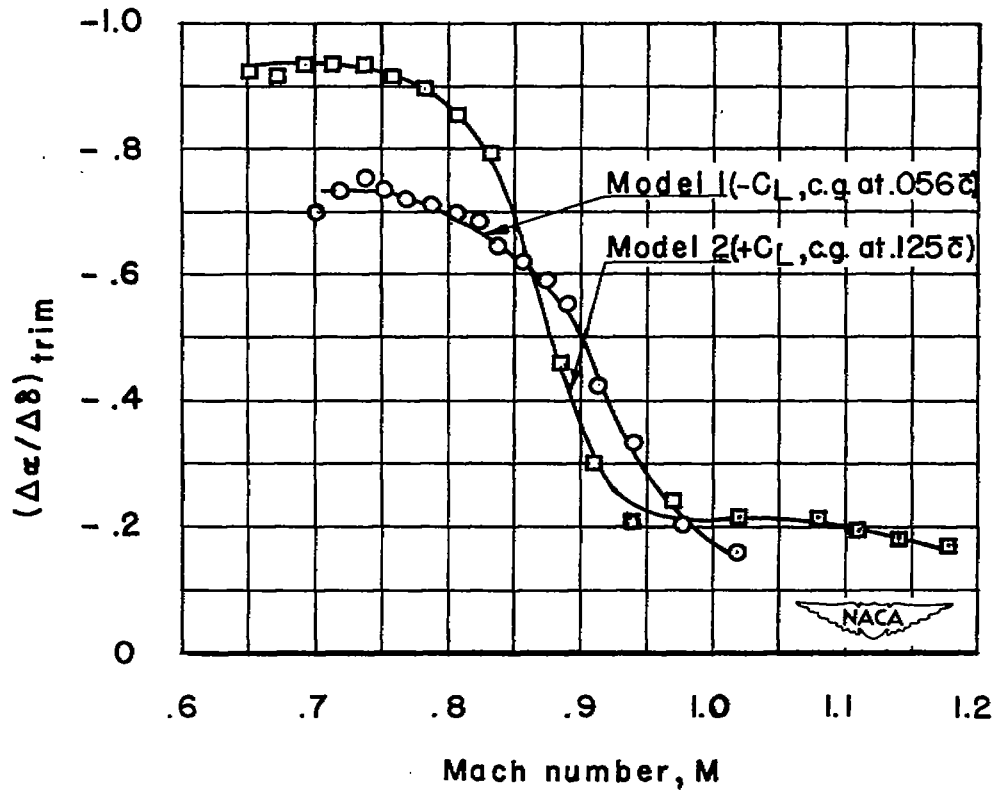


Figure 29.- Variation with Mach number of change in trim angle of attack with respect to elevator deflection.

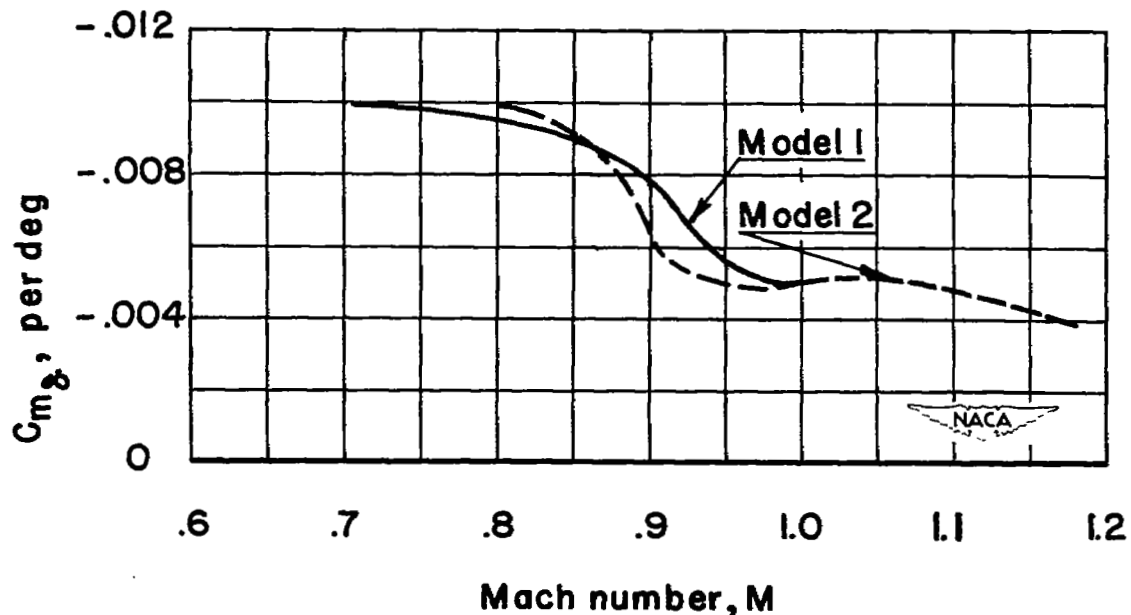


Figure 30.- Rate of change of pitching-moment coefficient with elevator deflection as a function of Mach number.

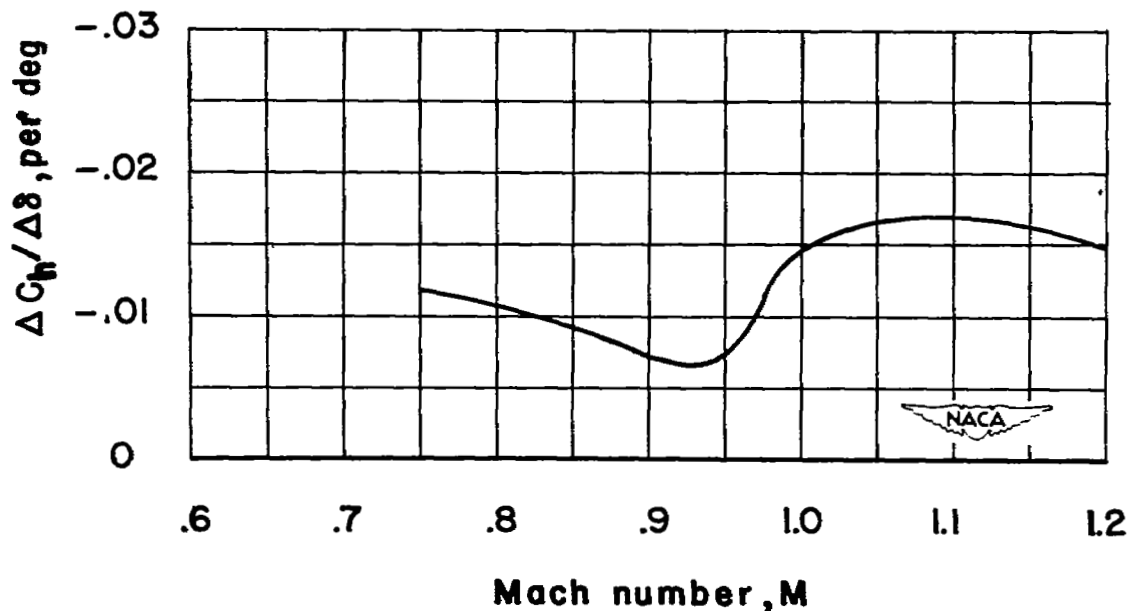


Figure 31.- Variation of elevator hinge-moment coefficient with elevator deflection as a function of Mach number, as obtained from model 2.

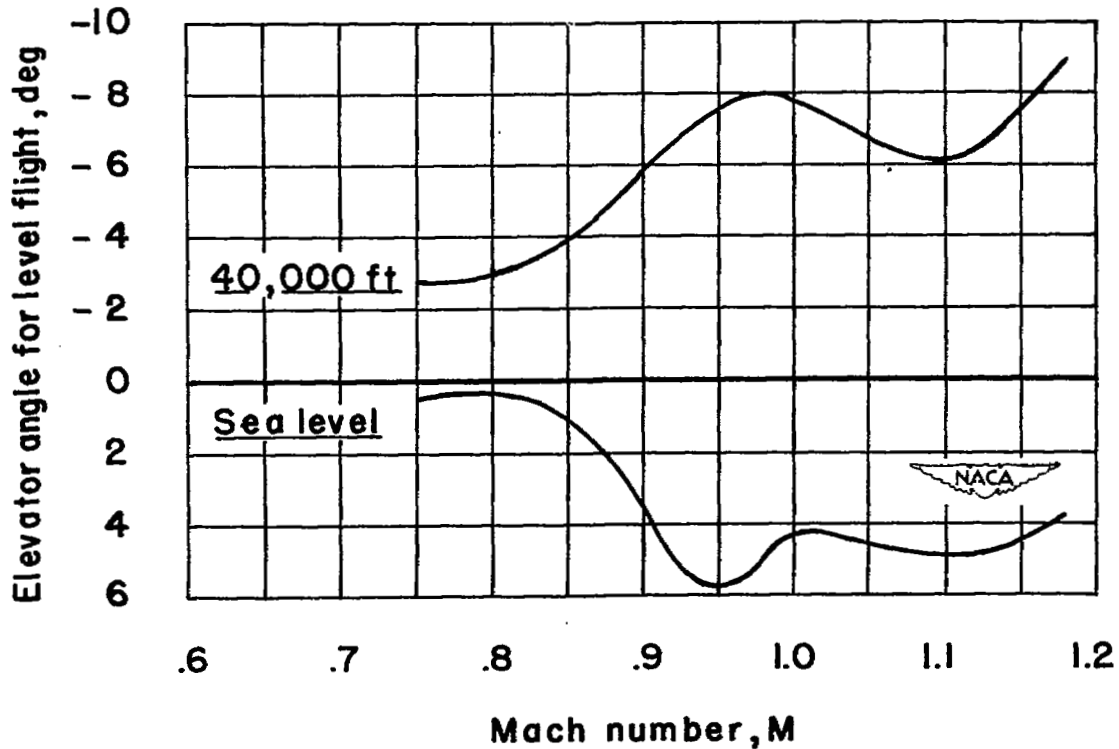


Figure 32.- Variation with Mach number of elevator angle required for the assumed full-scale airplane to maintain level flight. Center of gravity at $0.18\bar{c}$.

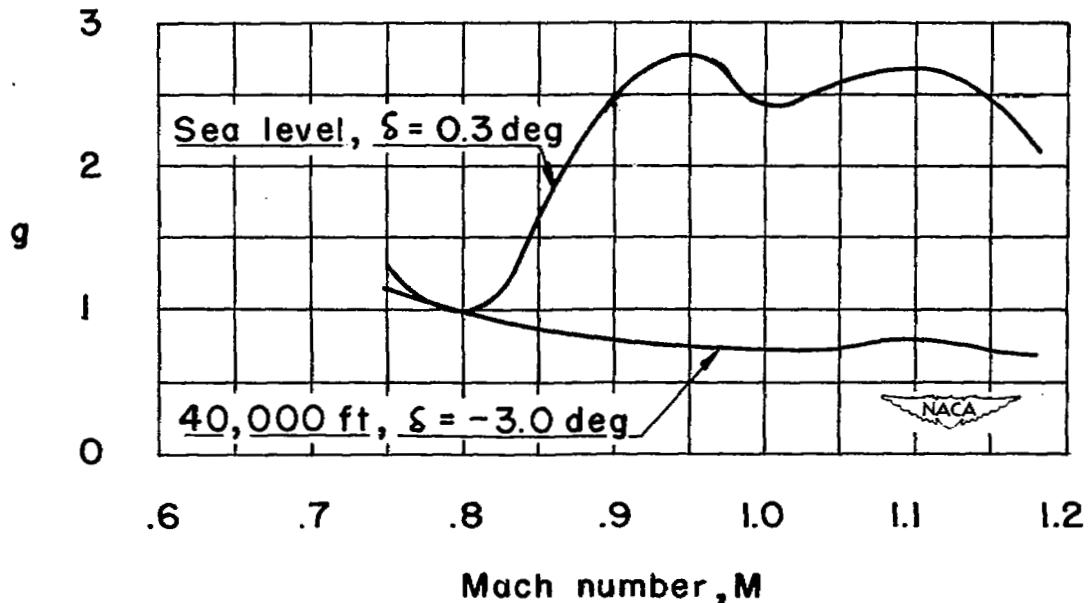


Figure 33.- Variation with Mach number of normal force developed at a constant elevator deflection for the assumed full-scale airplane. Center of gravity at $0.18\bar{c}$.

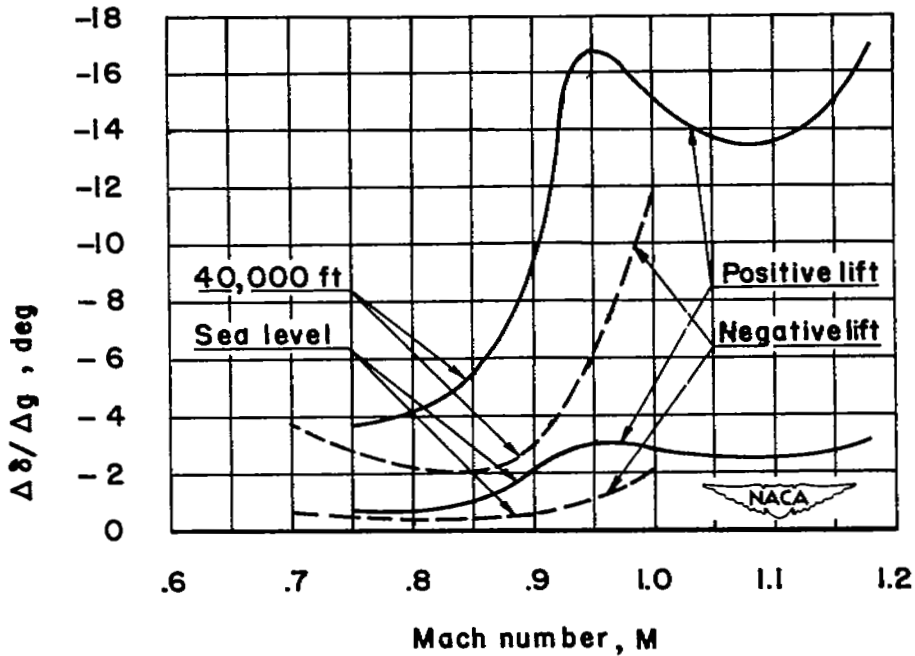


Figure 34.- Variation with Mach number of elevator deflection required per g for the assumed full-scale airplane. Center of gravity at $0.18\bar{c}$.

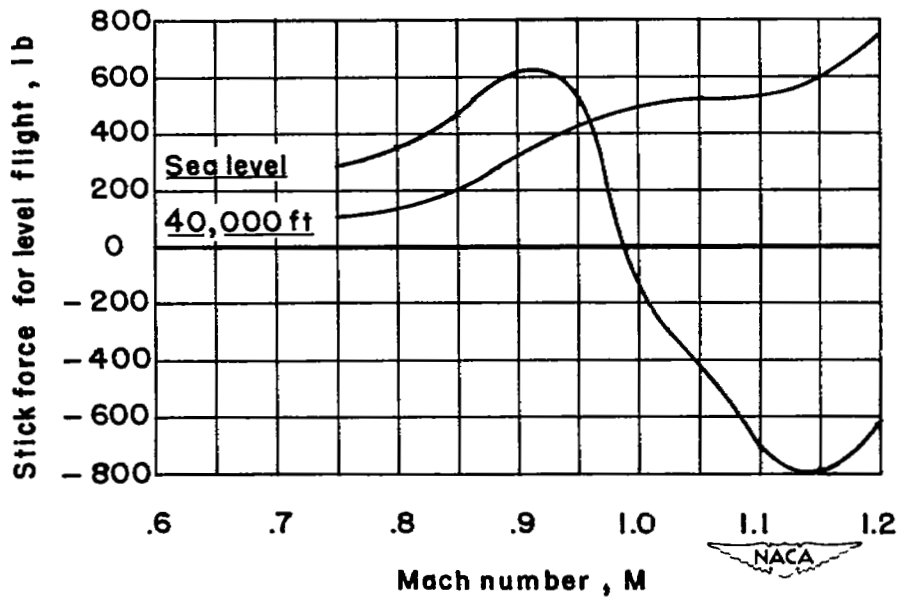


Figure 35.- Variation with Mach number of stick force required for the assumed full-scale airplane to maintain level flight. Center of gravity at $0.18\bar{c}$.

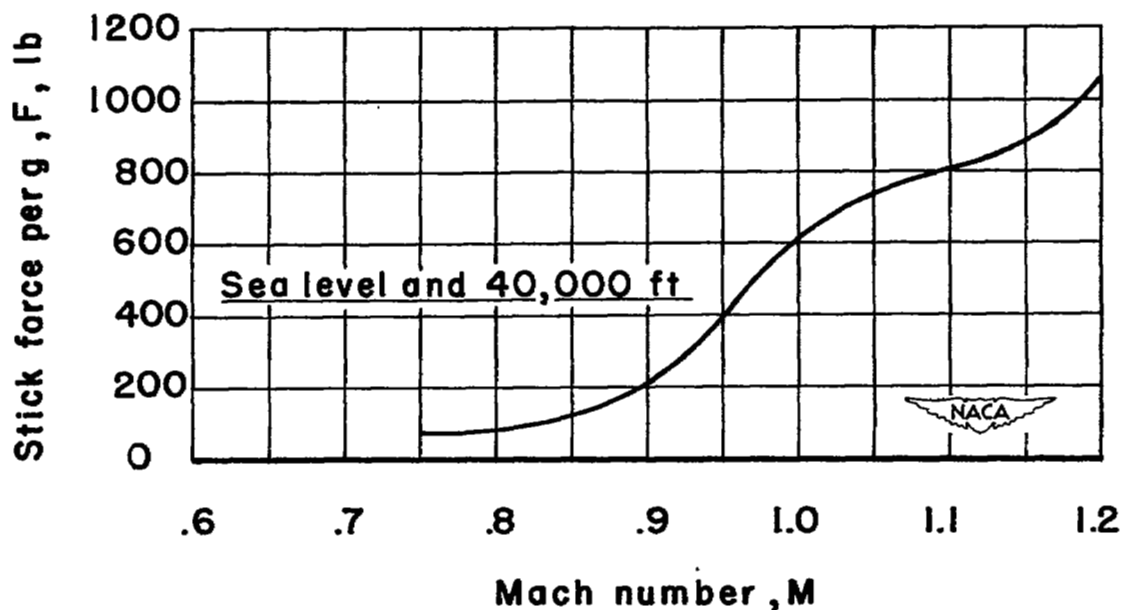


Figure 36.- Variation with Mach number of stick force required per g for the assumed full-scale airplane. Center of gravity at $0.18\bar{c}$.

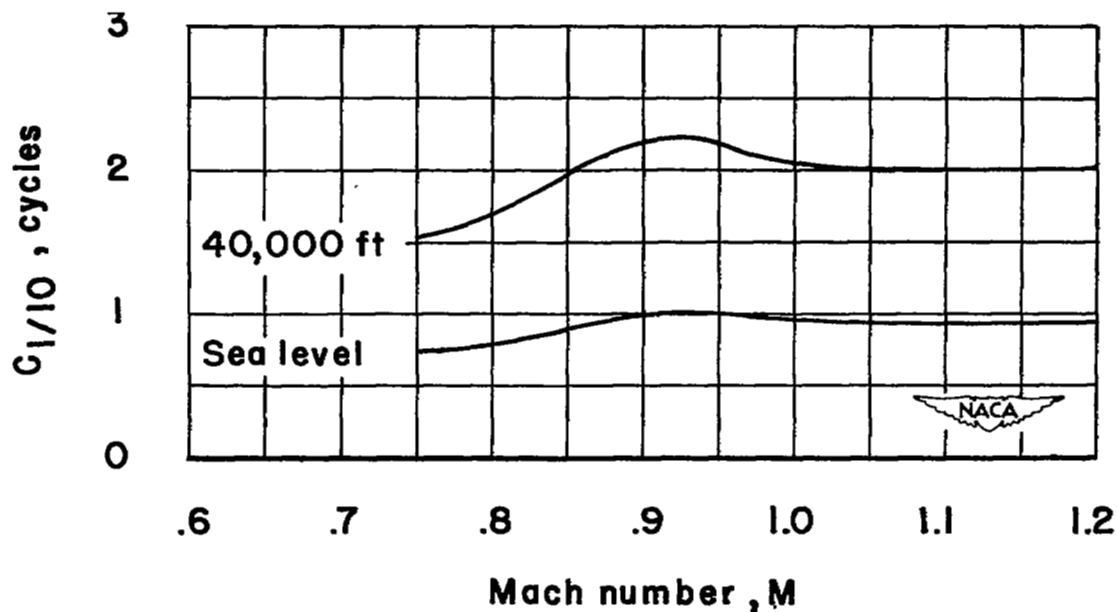


Figure 37.- Variation with Mach number of the cycles required for short-period longitudinal oscillation of the assumed full-scale airplane to damp to one-tenth amplitude. Center of gravity at $0.18\bar{c}$.

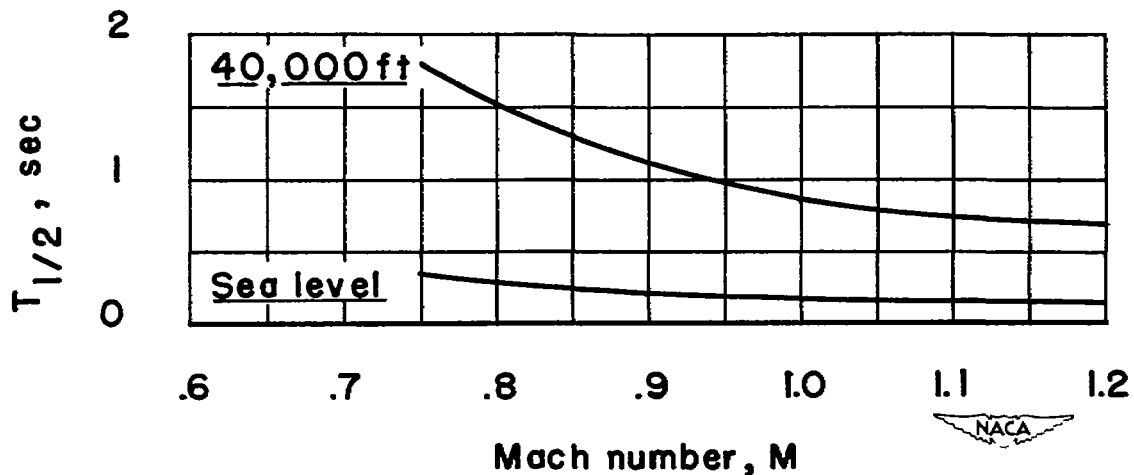


Figure 38.- Variation with Mach number of time required for short-period longitudinal oscillation of the assumed full-scale airplane to damp to one-half amplitude. Center of gravity at $0.18\bar{c}$.

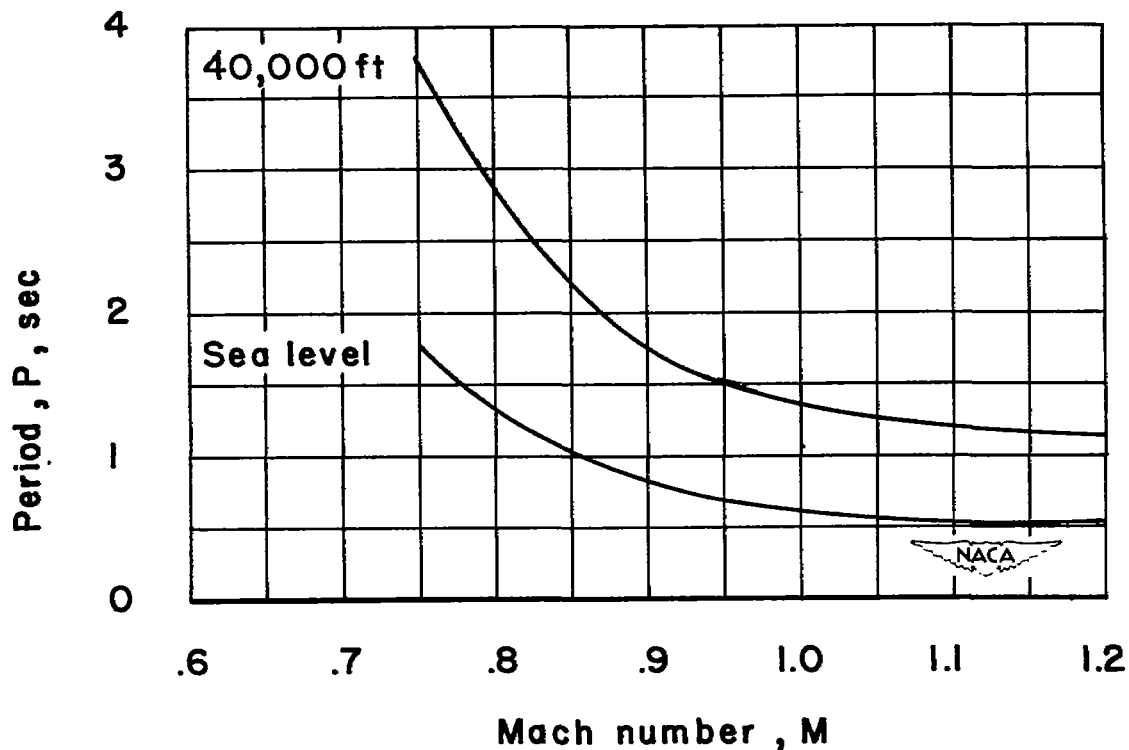


Figure 39.- Variation of period of longitudinal oscillation of the assumed full-scale airplane with Mach number. Center of gravity at $0.18\bar{c}$.

NASA Technical Library



3 1176 01436 8055

